NASA Contractor Report 189641

*p-56*

# SUBSONIC INVESTIGATIONS OF VORTEX INTERACTION CONTROL FOR ENHANCED HIGH-ALPHA AERODYNAMICS OF A CHINE FOREBODY/DELTA WING CONFIGURATION

Dhanvada M. Rao and M. K. Bhat

ViGYAN, INC.
Hampton, Virginia

# N/\S/\

National Aeronautics and
Space Administration

**Langley Research Center**
Hampton, Virginia 23665-5225

ERRATA

NASA Contractor Report 189641

Subsonic Investigations of Vortex Interaction Control
for Enhanced High-Alpha Aerodynamics of a Chine
Forebody/Delta Wing Configuration

Dhanvada M. Rao and M. K. Bhat

June 1992

Attached is a corrected copy of NASA Contractor Report 189641. Beginning with page 36, the wrong figures
were inadvertently printed in the report which was previously sent to you. Please destroy all copies of the
report that you previously received.

# SUBSONIC INVESTIGATIONS OF VORTEX INTERACTION CONTROL FOR ENHANCED HIGH-ALPHA AERODYNAMICS OF A CHINE FOREBODY/DELTA WING CONFIGURATION

by Dhanvada M. Rao and M.K. Bhat
VíGYAN, Inc.

## ABSTRACT

A proposed concept to alleviate high-alpha asymmetry and lateral/directional instability by decoupling of forebody and wing vortices was investigated on a generic chine forebody/ 60 deg. delta configuration in the NASA Langley 7- by 10-Foot High Speed Tunnel. The decoupling technique involved inboard leading-edge flaps of varying span and deflection angle. Six-component force/moment characteristics, surface pressure distributions and vapor-screen flow visualizations were acquired, on the basic wing-body configuration and with both single and twin vertical tails at $M_\infty$ = 0.1 and 0.4, and in the range $\alpha$ = 0 to 50° and $\beta$ = -10° to +10°. This report presents results highlighting the potential of vortex de-coupling via leading-edge flaps for enhanced high-alpha lateral/directional characteristics.

## SYMBOLS & ABBREVIATIONS

Force and moment data presented in this paper have been reduced to conventional coefficient form based on the wing trapezoidal planform area (extended to the fuselage centerline). Moments are referenced to the balance center. All dimensional values are given in U.S. Customary Units. The symbols are defined as follows:

| | | | |
|---|---|---|---|
| b | wing span, 19.20in | S | wing planform reference area, 208.224 in$^2$ |
| $C_L$ | lift coefficient, Lift/qS | Y | spanwise distance from model centerline, in. |
| $C_l$ | rolling moment coefficient, Rolling moment/qSb | $\alpha$ | angle of attack, deg. |
| $C_m$ | pitching moment coefficient, Pitching moment/qSc | $\beta$ | angle of sideslip, deg. |
| $C_n$ | yawing moment coefficient, Yawing moment/qSb | C.V.T. | central vertical tail |
| $C_p$ | pressure coefficient | LEF | leading-edge flap |
| c | mean geometric chord of reference wing panel, 10.92in | V.T. | vertical tail |
| $M_\infty$ | free-stream Mach number | T.T. | twin tail |
| q | free-stream dynamic pressure | | |

1

# INTRODUCTION

The beneficial interaction of forebody chine vortices with the leading-edge separated flowfield of highly-swept delta wings is known (see refs. 1, 2) to significantly improve the maneuvering lift capability in the moderate to high-alpha range. When the coupled chine-wing vortices eventually break down, however, severe stability and handling difficulties arise in the presence of sideslip, and result in configurations prone to roll departure. A concept of controlled vortex decoupling to alleviate these problematical near-stall and post-stall aerodynamics was proposed and subjected to an exploratory low-speed tunnel investigation (ref. 3). That precursor study demonstrated the feasibility of maintaining a decoupled vortex system up to high angles of attack and sideslip on a generic, close-coupled chine-delta configuration. Inboard leading-edge flap deflection was found to be particularly effective for this purpose, resulting in beneficial post-stall characteristics, viz., pitch-down and lateral/directional stability in the $C_{L,MAX}$ region and reduced vertical-tail buffet at high angles of attack.

Based as they were on data obtained with simplified flat-plate type model geometry at modest Reynolds number, the encouraging preliminary results of ref. 3 needed verification on a more realistic configuration (e.g., with blended chines and wings with realistic airfoils), and at higher Reynolds numbers. This report documents a test entry performed in NASA Langley Research Center 7- by 10-Foot High Speed Tunnel using a generic chine forebody/delta wing model, specifically designed for vortex decoupling investigations utilizing leading-edge flaps. The objectives of this test were to (1) verify the

2

concept, and acquire subsonic aerodynamic trends at high angles of attack and in sideslip; (2) generate a comprehensive data base of six-component force/moment and surface pressures useful for future CFD validation; (3) perform off-surface (vapor screen) visualizations of representative decoupled vortex architectures; and (4) attempt evaluation of vertical tail dynamic load alleviation potential of vortex decoupling.

The scope of this report comprises model description, test plan and procedures, summary of test configuration matrix and types of data acquired, discussion of the significant results and trends supported by selected data sets, and the main conclusions.

## MODEL AND FACILITY

The test model, shown in fig.1, has the following pertinent features:

(1)   A 60° cropped-delta planform incorporating NACA 65-005 airfoil modified with double-arc section forward of the maximum thickness and sharp leading edges.

(2)   Full-span leading edge flaps divided into three equal span segments, the inner two segments being deflectable downwards at 10, 20 or 30 deg. on independent brackets.

(3)   Alternate arrangements of single-central and twin-outboard vertical tails with $t/c = .05$ symmetrical double-wedge airfoil sections, each tail instrumented with root-bending moment strain gage bridges;

(4)   The central fuselage section accommodating a NASA Langley six-component strain gage balance (# 754)

(5)   A total of 276 static orifices grouped in six stations with three forebody and three wing (upper surface) spanwise rows. The hollow forebody housed three electronically scanned pressure (ESP) modules, and additional three were located downstream of the model sting. The aft three modules required bridging the balance with about 140 flexible pressure tubes; the offsets in

3

balance outputs resulting from this bridging were measured and judged insignificant for the purpose of this test.

A photograph of the model mounted in the test facility is shown in fig. 2.

The tests were conducted in NASA Langley 7- by 10-Foot High Speed Wind Tunnel, which is a closed-return, atmospheric facility (see ref. 4 for a description of the facility). The model was supported on a 'high-alpha' sting system having a roll-positioning capability to obtain prescribed combinations of alpha and beta angles. The humidity level in the test-section was modulated via flow temperature control and water injection, in order to optimize flow condensation around the model for vapor-screen visualizations. During data measurement tests however, the water injection was turned off and condensation-free flow conditions were maintained about the model. A laser-generated light-sheet system was utilized, whose rotation allowed the plane of illumination to be axially translated over the model length. The cross-plane visualization was viewed with a sting-mounted video camera located behind the model and also a camera external to the test section, aft of the model and to the right.

The basic elements of the test program comprised alpha sweeps at ß = 0°, 5° and -5°, and beta sweeps between -10° and 10° at alpha of 20°, 30° and 40° (nominal). The free-stream Mach numbers were 0.1 and 0.4, and Reynolds numbers (based on mean aerodynamic chord) of $0.6 \times 10^6$ and $2.24 \times 10^6$, respectively. The test configurations and Mach numbers are indicated in the Table I.

For each of the above test cases, the following measurements were made: (1) six-component forces and moments; (2) surface pressures at six model stations; and (3) vertical tail root-bending moment signals. However, the low signal-to-noise ratio in the tail gage outputs prevented acquisition of useful data in this test entry; presentation and discussion of tail dynamic characteristics will be deferred to a later report.

## RESULTS AND DISCUSSION

### 1. TAIL-OFF CHARACTERISTICS AT ZERO BETA

The baseline configuration refers to the case without vertical tails or flap deflection. The force and moment results of $\beta = 0°$ alpha sweeps including lift and the moment coefficients, in the range $\alpha = 0°$ to $50°$ are shown in fig. 3, for both $M_\infty = 0.1$ and 0.4. A sharply-peaked $C_{L,MAX}$, followed by abrupt lift loss and concurrent pitch-up, are indicative of vortex breakdown onset on the wing surfaces. In comparing data for the two Mach numbers, a four-fold increase of Reynolds number between $M_\infty = 0.1$ and 0.4 is believed to predominate over the compressibility effects in the stall region. A somewhat earlier stall together with a sharp, localized roll disturbance found at the lower Reynolds number would indicate an asymmetric collapse of lift on the two wing panels. This characteristic may be due to transitional viscous effects on the vortex-induced secondary separation; a lack of significant roll input in the data at higher Reynolds number suggests that vortex breakdown occurs symmetrically on both sides.

5

## 2. TAIL-OFF CHARACTERISTICS WITH SIDESLIP

Beta-sweep results at $\alpha = 20°$, $30°$, and $40°$ (nominal angles) on the baseline yawing and rolling moments are presented in fig.4. At $\alpha = 30°$ (i.e., approaching $C_{L,MAX}$) a pronounced sensitivity is noted with respect to small sideslip angles, particularly in the rolling moment data. Although a stable trend is established at higher beta angles, the rolling-moment discontinuity and reversal across $\beta = 0°$ presages aircraft control and handling difficulties. Some insight into this phenomenon is provided by the spanwise pressure distributions at $\alpha = 30°$ and in the vicinity of $\beta = 0°$ measured during a beta-sweep test (fig. 5). These results show a rapid switch of the spanwise asymmetry (induced by vortex breakdown on the windward panel) within a very small sideslip increment on either side of $\beta = 0°$, which is responsible for the discontinuous roll reversal. This type of rolling moment sensitivity with respect to $\beta$ had been previously observed during the investigations of ref. 3. The lateral/directional characteristics at $\alpha = 40°$ regain a continuous and stable trend through $\beta = 0°$, indicating that a total and symmetrical vortex breakdown prevails on both the wing panels in this sideslip range.

## 3. EFFECT OF VERTICAL TAILS

The addition of a central vertical tail has no noticeable effect on the baseline $\beta = 0°$ aerodynamics, as shown in fig. 6. On the other hand, the twin-tails have profound and adverse influence on the lift and stall characteristics. The wing-mounted verticals apparently interfere directly with the chine-wing vortex system that is the dominant lift mechanism on the test configuration. The maximum lift attained on the twin-tail configuration is about

6

equal to the post-stall lift in the baseline (or central tail) case, which suggests that the wing-mounted tails induce a premature breakdown of the wing vortices. The spanwise pressure distributions presented.in figs. 7A, 7B and 7C show a collapse of vortex-induced suction peaks at station #5, caused by an upstream propagation of vortex breakdown forced by the twin tails. At the spanwise station #6 (i.e., intersecting the tails), a uniform suction pressure occurs outboard of the tails which indicates a fully stalled wing flow. This outboard wing separation could be triggered by the stalling of twin tails due to a pronounced side-wash induced by the chine vortices.

The influence of twin tails on the beta characteristics is shown in fig. 8. The twin tails are found to improve directional stability at the larger sideslip angles, presumably due to higher dynamic pressures prevailing at the wing-mounted verticals than at the center tail. The roll sensitivity across $\beta = 0^\circ$ of the tail-off and central-tail configurations at $\alpha = 30^\circ$ is notably absent with the twin tails; instead, a continuous stable trend is obtained. These results suggest that the twin tails force a fundamental restructuring of the vortex-coupling behavior of the basic chine-wing configuration.

## 4. LEADING EDGE FLAPS

**Vertical Tail Off Characteristics:** The results of 2/3-span leading edge flap at 30 deg. deflection on the tail-off configuration, presented in fig. 9, provide a first indication of vortex decoupling effect on the high-alpha characteristics. The alpha-sweep data show that the leading-edge camber due to flaps mainly affects the lift curve by reducing the vortex lift contribution; however there is only a small $C_{L,MAX}$ penalty.

A noteworthy effect of flap deflection, observed in the beta sweep results at $\alpha = 34°$ (fig. 10), is the elimination of the critical roll-sensitivity of the basic configuration, which is replaced by a smoother and more tractable lateral trend across $\beta = 0°$. It would appear that the transition between burst and decoupled vortex states with deflected flaps is smooth and continuous as the sideslip reverses sign, unlike the abrupt switching between two bistable states occurring on the basic configuration.

**Central Vertical Tail Characteristics:**     Spanwise pressure distributions at $\alpha = 30°$ showing the effect of 2/3-span leading edge flaps are presented in fig. 11. The suction peaks at station # 5 indicate that the decoupled wing vortices have moved outboard to the flaps. The effects of 2/3-span leading-edge flaps are clearly seen in the central-tail lateral/directional characteristics from alpha-sweeps at $\beta = \pm 5°$ (fig.12). Both the stability parameters are significantly enhanced in the range $\alpha = 20°$ to $30°$ where the $0°$ LEF configuration suffers a pronounced lateral stability loss.

Beta-sweep results with $30°$ deflected 2/3-span flaps, presented in fig.13, show that at $\alpha = 23.3°$ the directional and lateral stability are improved across the sideslip range; at $\alpha = 34.3°$, the main result is to alleviate the $\beta = 0°$ roll sensitivity. At a higher angle of attack $(45.1°)$ the flap effect is essentially lost. The effect of increasing deflection of the 2/3-span LEF as shown in fig.14, is mainly to improve the roll sensitivity at $\alpha = 34°$.

The effect of flap-span reduction from 2/3 to 1/3, at a constant deflection of $30°$, is shown in fig. 15. This comparison was intended to provide some indication of the relative importance of vortex decoupling versus wing flow improvement due to leading edge

deflection, with respect to near-stall lateral/directional stability benefits. The reduced-span flaps are seen to produce essentially the same improvements in the $C_n$ and $C_l$ characteristics, which supports the effectiveness of the decoupling mechanism. A comparison of the spanwise pressure distributions at $\alpha = 30°$ with 1/3-span and 2/3-span LEF (fig. 16) shows both to generate virtually identical wing pressure fields.

**Twin Vertical Tail Characteristics:** As already pointed out, the twin-tail configuration produces quite different high-alpha characteristics by forcing a pre-mature bursting of the vortices, thus preventing the classical interaction and chine/wing vortex merger as found on the tail-off and central-tail configurations. Consequently, flap deflection has little effect on the $\beta = 0°$ lift and moment characteristics, as shown in fig. 17. For the same reasons, the twin-tail configuration remains laterally and directionally stable through the alpha range, as indicated in the $\beta$ sweep results of fig. 18. The leading-edge flap deflection in this case produces little additional lateral/directional benefits.

## VAPOR-SCREEN FLOW VISUALIZATIONS

Selected still frames from the videos taken looking upstream with the sting-mounted camera during sweeps of the laser sheet, with the light sheet positioned between wing stations #5 and #6, are presented in support of a discussion of the vortical characteristics of the different model configurations. The free-stream Mach number corresponding to these visualizations was 0.4. Note that the humidity level was not regulated, which may be responsible for varying condensation and, consequently, the contrast achieved in the different visualizations. Note also that the photographs were hand notated with the nominal value of $\alpha$. The actual values are typed alongside the photograph.

(i)   **VT off; 0° LEF:**   An alpha sequence at ß = 0° is shown in fig. 19.  At α = 23° the chine and wing vortices remain distinct, but at α=34° become strongly coupled as well as non-symmetrical.  At α = 43° (i.e., past $C_{L,MAX}$), the stalled flowfield shows remnant vortical structures in a relatively symmetric, post-breakdown pattern.

(ii)   **VT off; 2/3-Span 30° LEF:** A comparable alpha-sequence at ß = 0° indicating the main effects of 30° flap deflection is shown in fig. 20.  The uncoupled flowfield at α = 23° is little different from the baseline case.  The α = 34° case however is dramatically altered, with the chine and wing vortices remaining well apart and in a symmetrical pattern.  At α = 45° the stalled flow on the wing remains vortically structured and better defined than in the baseline case; however, the effect of varying light and vapor condensation conditions between the two test cases cannot be ruled out.

(iii)   **CVT; 0° LEF:**   The alpha sequence shown in fig. 21 allows the central-tail effects to be assessed in relation to baseline configuration.  These visualizations show that addition of central tail does not materially alter the wing flow development through stall, in corroboration with the force/moment and pressure distribution results already noted.

(iv)   **CVT; 2/3-Span 30° LEF:**   Application of 30° deflected 2/3-span leading-edge flaps on the central vertical tail configuration (fig. 22) produces decoupling effects that are essentially similar to those already noted on the tail-off

configuration. The chine vortices appear to stay clear off the central tail on either side up to $\alpha = 40°$, which should be favorable for tail buffet alleviation.

(v) **CVT: 1/3-Span 30° LEF:** The reduced 1/3-span leading-edge flaps generate wing flow structures quite similar to those observed with 2/3-span LEF in the range $\alpha = 20°$ to 40°, as shown in fig. 23. The vortex decoupling effectiveness of the reduced-span LEF is clearly demonstrated in the visualization at $\alpha = 30°$.

(vi) **CVT in Sideslip :** A comparison of the baseline and 2/3-span leading-edge flap cases, at $\alpha = 30°$, $\beta = 4°$, is presented in fig. 24. On the leeward side, flap deflection is seen mainly to diminish the leading edge vortex with relatively little change in the chine vortex position. On the windward wing, however, a well organized and apparently uncoupled vortical structure replaces the featureless region of the baseline case. This implies increased vortical lift on the windward panel with associated stabilizing rolling moment, consistent with the force/moment results.

(vii) **Twin Tails: 0° LEF:** As seen in fig. 25, the wing vortices are burst prematurely in the presence of twin tails at $\alpha = 23°$. The chine vortices lie inboard of the tails and are little affected. The wing flow at $\alpha = 34°$ appears to be stalled primarily due to chine vortex breakdown, although symmetry is retained unlike the central tail configuration. At $\alpha = 45°$, a symmetrical chine vortical structure persists between the tails.

(viii)  **Twin Tails: 2/3-Span 30° LEF:**  Leading-edge flap deflection mainly suppresses the wing vortices on the twin-tail configuration, shown by the visualization results in fig. 26. Comparison with the 0° LEF case (fig. 25) suggests that at $\alpha$ = 34° the chine vortices continue unburst as they pass between the tails.


## CONCLUSIONS

A subsonic wind tunnel investigation was performed on the efficacy of inboard leading-edge flaps to achieve chine-wing vortex decoupling at high angles of attack, and its consequent aerodynamic benefits to a close-coupled forebody chine/delta wing configuration. The main results of the study, based on force/moment and wing upper-surface pressure measurements and vapor-screen flow visualizations, can be summarized as follows:

(1)  The tail-off configuration stalls abruptly at about $\alpha$ = 34° due to bursting of the interacting chine/wing vortices. Approaching $C_{L,MAX}$, (and into the post-stall regime) the configuration not only becomes laterally unstable but also extremely roll-sensitive near zero beta.


(2)  Inboard 2/3-span, 30° deflected leading-edge flaps produce decisive effects on the lateral characteristics, most importantly the elimination of $\beta = 0°$ roll sensitivity and improvement of lateral stability in the vicinity of $C_{L,MAX}$, which itself is not significantly penalized.

12

(3)     Inboard leading-edge flaps of 1/3-span are nearly as effective as the 2/3-span LEF, indicating that vortex decoupling is the essential mechanism underlying enhanced high-alpha lateral aerodynamics, further assisted by flow improvement over a larger span of the wing.

(4)     Addition of a central vertical tail leaves the baseline high-alpha longitudinal and lateral characteristics virtually unchanged; it also has no effect on the vortex decoupling capability of the leading-edge flaps.

(5)     Attempts during this test to evaluate tail dynamics were unsuccessful due to high noise level in the data; flow visualizations however suggest that vortex decoupling improves the high-alpha flow environment at the central tail location which should be favorable to tail buffet alleviation.

(6)     Wing-mounted twin tails profoundly affect the delta wing vortex evolution (presumably by forcing premature bursting), which prevents the development of classical chine/wing vortex interactions. This significantly reduces the maximum lift capability but also eliminates the high-alpha lateral instability.

## ACKNOWLEDGEMENTS

## REFERENCES

1. Erickson, G. E., and Brandon, J. M.: " Low-Speed Experimental Study of the Vortex Flow Effects of a Fighter Forebody Having Unconventional Cross-Section ". AIAA paper 85-1798-CP, 1985.

2. Hall, R. M., and DelFrate, J. H.: " Interaction Between Forebody and Wing Vortices, A Water Tunnel Study ". AFWAL-TM-85-252, 1986.

3. Rao, Dhanvada M., and Bhat, M. K.: " A Low-Speed Wind Tunnel Study of Vortex Interaction Control Techniques on a Chine-Forebody/Delta-Wing Configuration." NASA CR-189616, 1992.

4. NASA: " Aeronautical Facilities Catalogue ", NASA RP-1132, Vol. 1, page 79A, January 1985.

TABLE I
Test Model Configurations and Mach Numbers

| Case | Vertical Tail | | | LEF Span | | LEF Deflection deg. | | | | Mach No. | |
|---|---|---|---|---|---|---|---|---|---|---|---|
| | Off | CVT | TT | 1/3 | 2/3 | 0 | 10 | 20 | 30 | 0.1 | 0.4 |
| 1 | X | | | | | X | | | | | X |
| 2 | X | | | | X | | X | | | | X |
| 3 | X | | | | X | | | X | | | X |
| 4 | X | | | | X | | | | X | | X |
| 5 | X | | | | | X | | | | X | |
| 6 | X | | | | X | | X | | | X | |
| 7 | X | | | | X | | | X | | X | |
| 8 | X | | | | X | | | | X | X | |
| 9 | | X | | | | X | | | | | X |
| 10 | | X | | | X | | X | | | | X |
| 11 | | X | | | X | | | X | | | X |
| 12 | | X | | | X | | | | X | | X |
| 13 | | X | | X | | | | | X | | X |
| 14 | | X | | | | X | | | | X | |
| 15 | | X | | | X | | X | | | X | |
| 16 | | X | | | X | | | X | | X | |
| 17 | | X | | | X | | | | X | X | |
| 18 | | | X | | | X | | | | | X |
| 19 | | | X | | X | | | X | | | X |
| 20 | | | X | | X | | | | X | | X |
| 21 | | | X | X | | | | | X | | X |

15
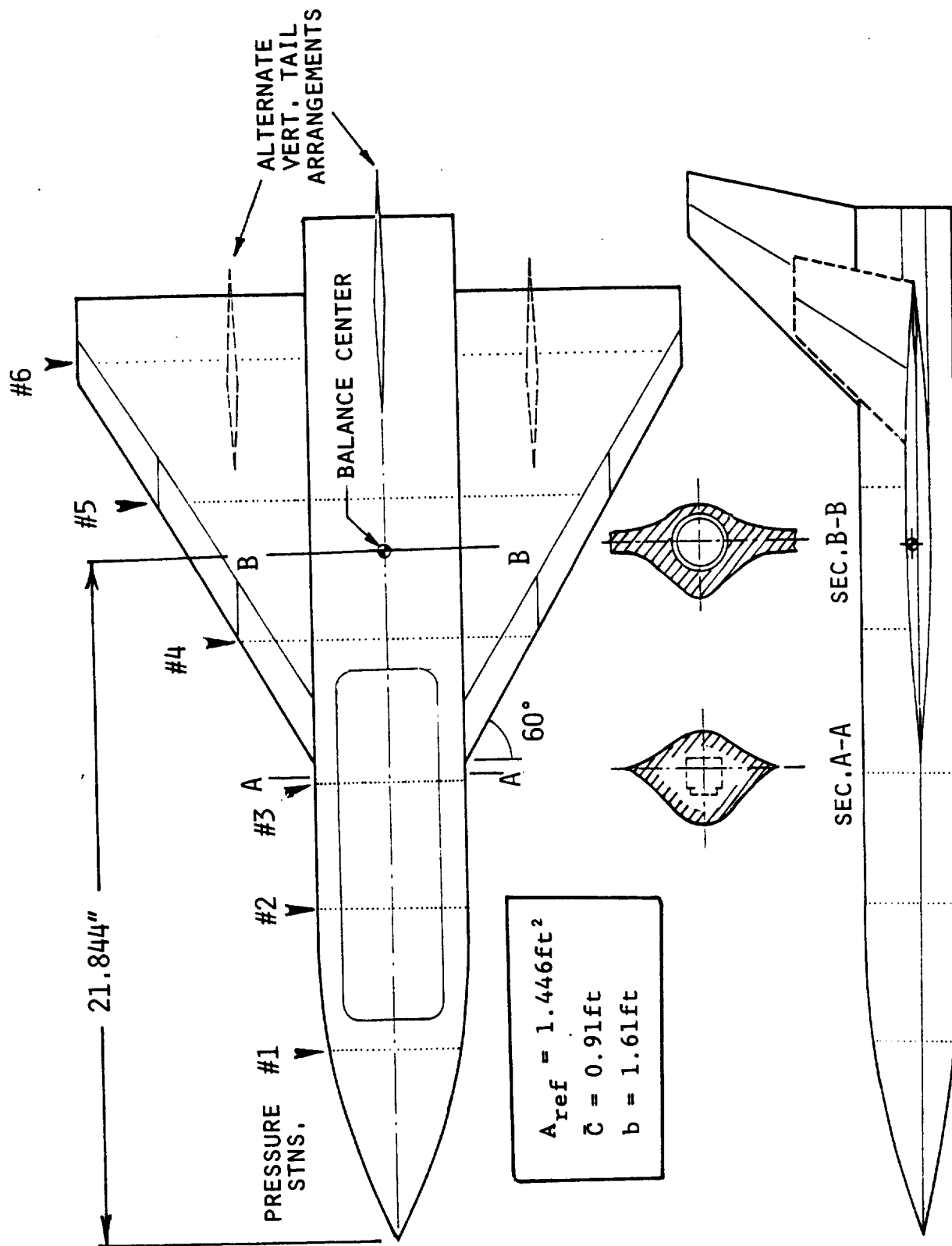
Fig. 1    Test model geometry

16
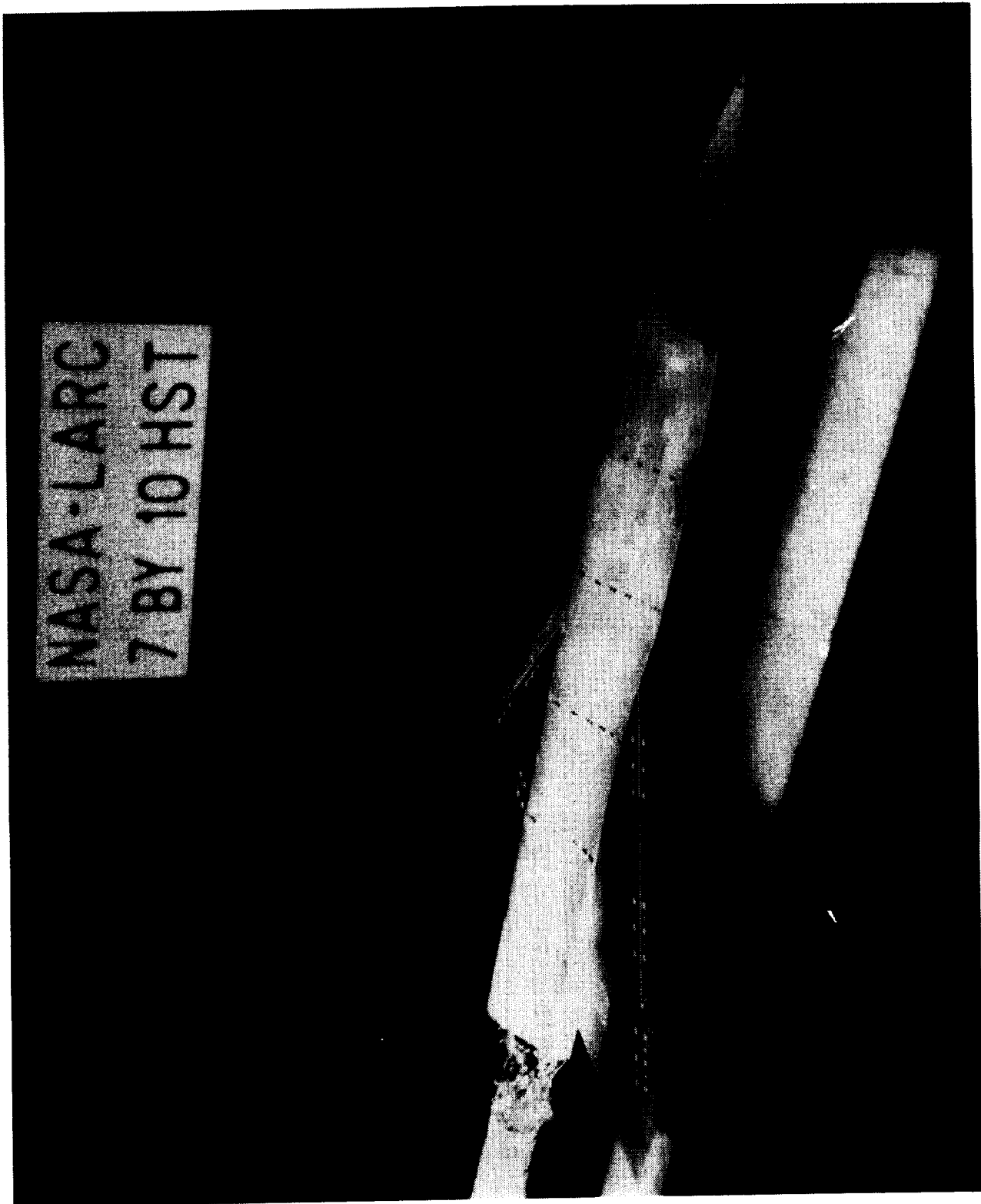
Fig. 2    Photograph of model mounted in LRC 7- by 10-Foot High Speed Tunnel (showing tail-off, 0° LEF configuration).
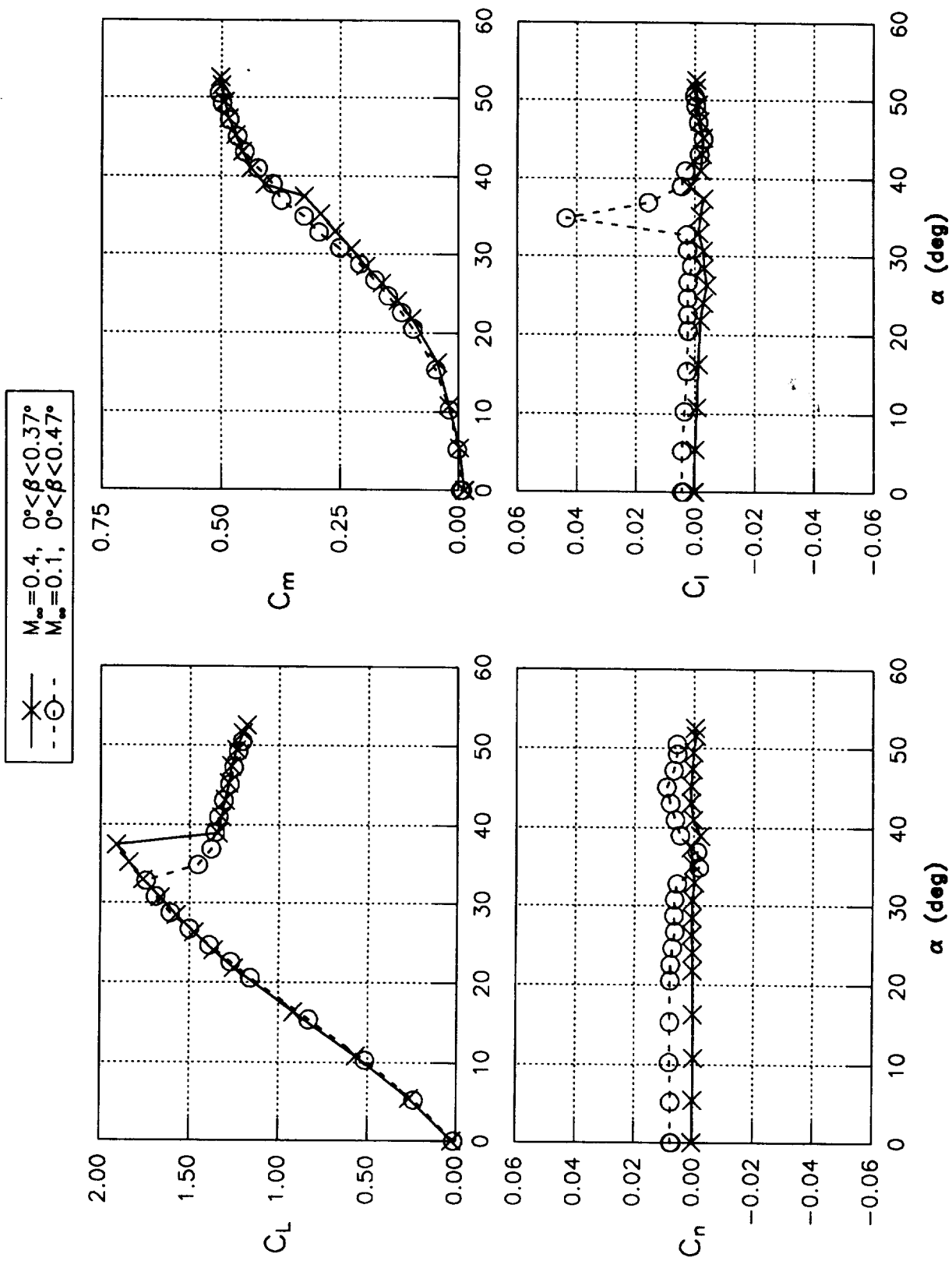
**Fig. 3** Lift and pitching/yawing/rolling moments versus angle of attack: tail off, 0° LEF configuration. ($M_\infty$ = 0.1 and 0.4).

18
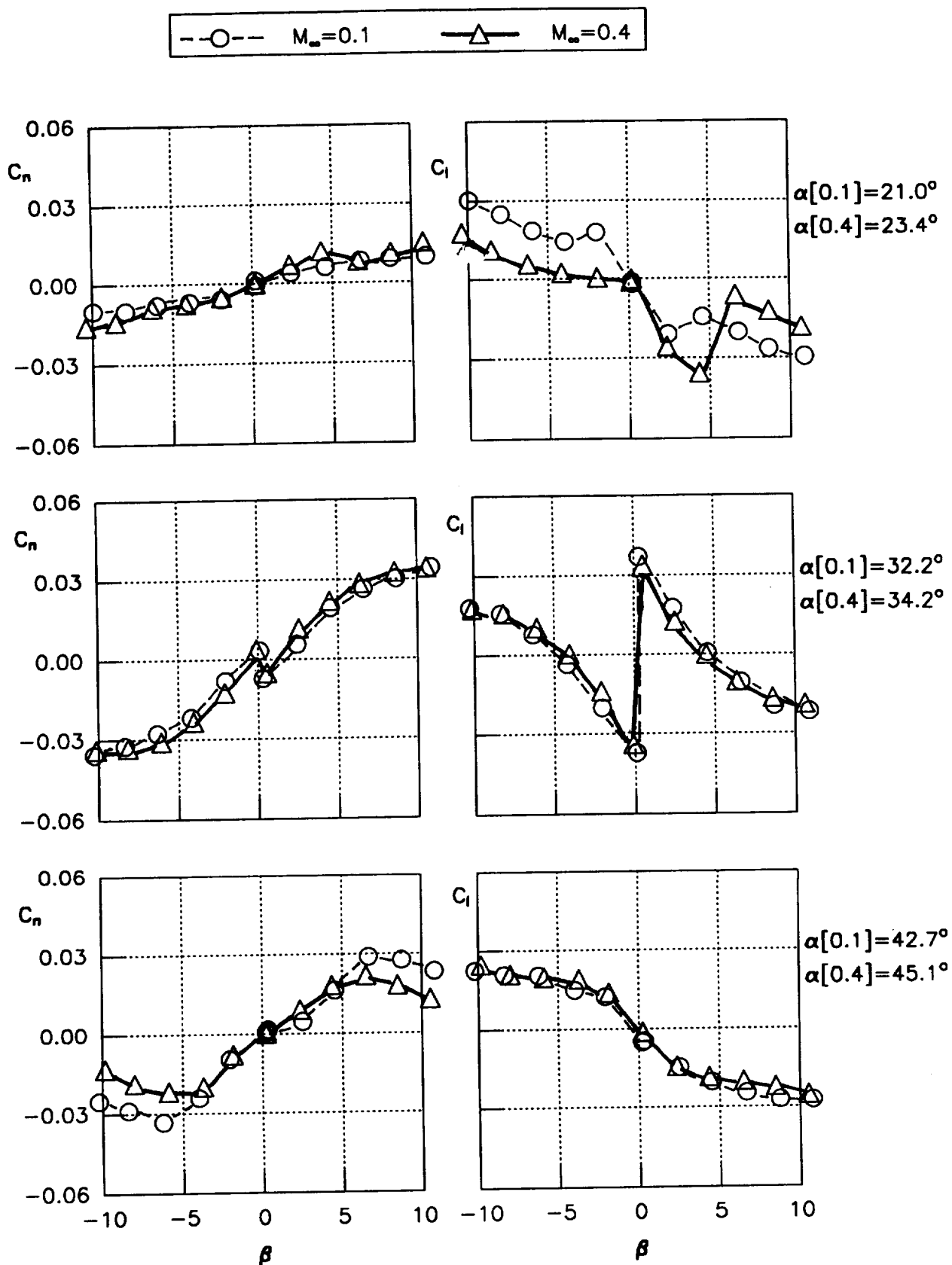
Fig. 4    Yawing and rolling moments versus sideslip at various angles of attack; tail off, 0° LEF configuration, M∞ = 0.1 and 0.4.
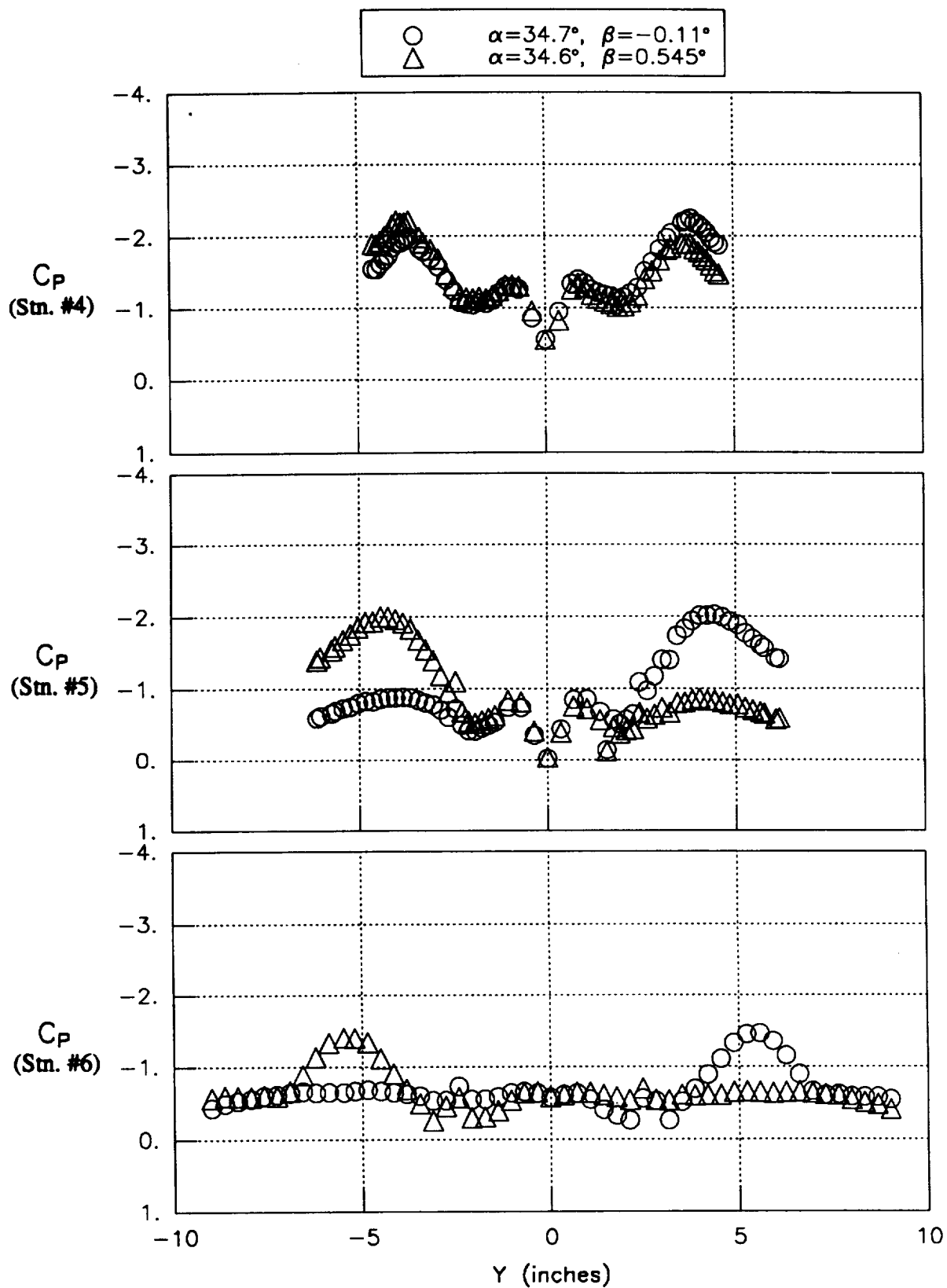
Fig. 5 Spanwise wing pressure distributions at small sideslip and $\alpha$ = 34°; tail off, 0° LEF configuration, $M_\infty$ = 0.4.
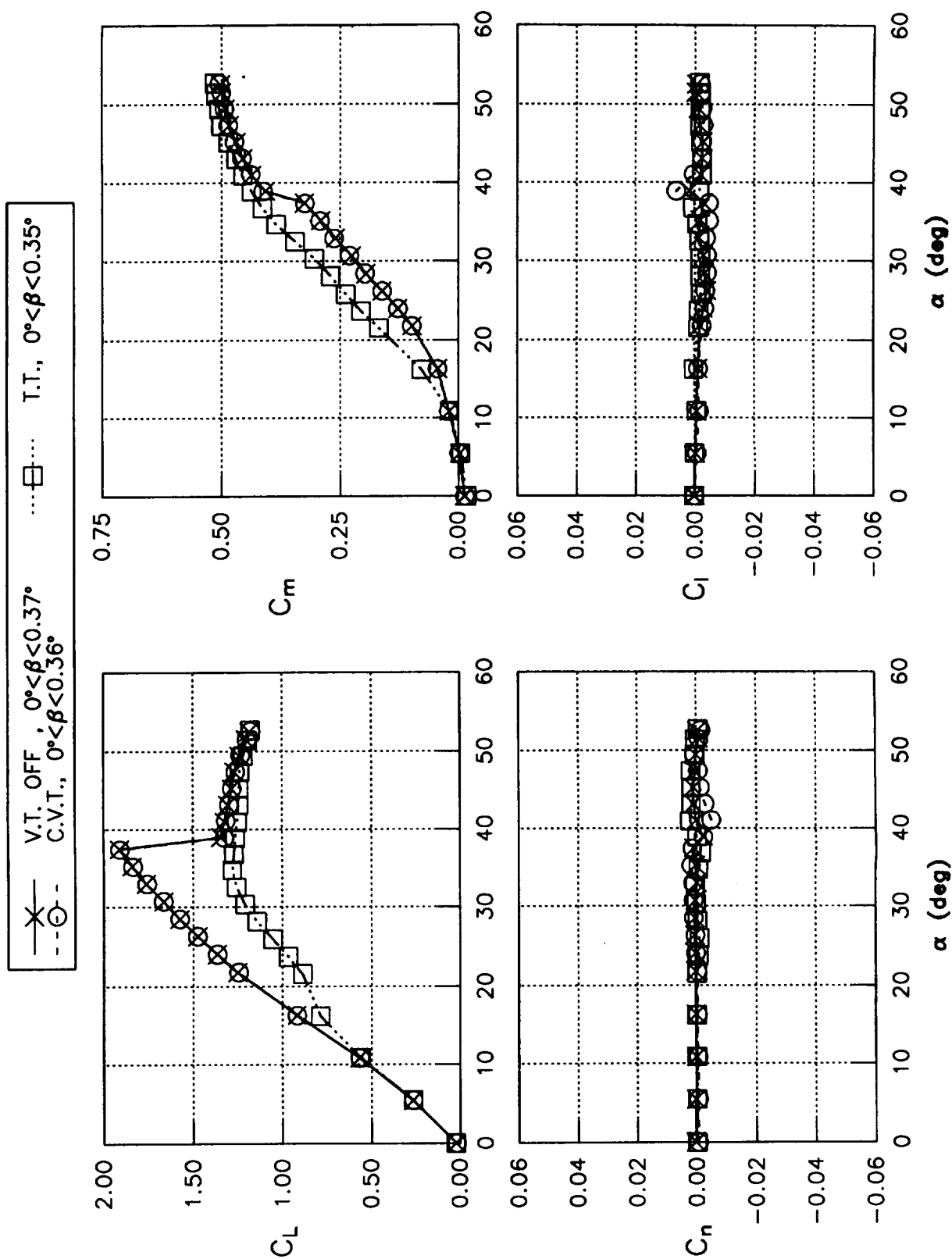
Fig. 6    Lift and moment coefficients versus angle of attack with 0° LEF; comparison of tail off, central-tail and twin-tail configuration, $M_\infty = 0.4$.
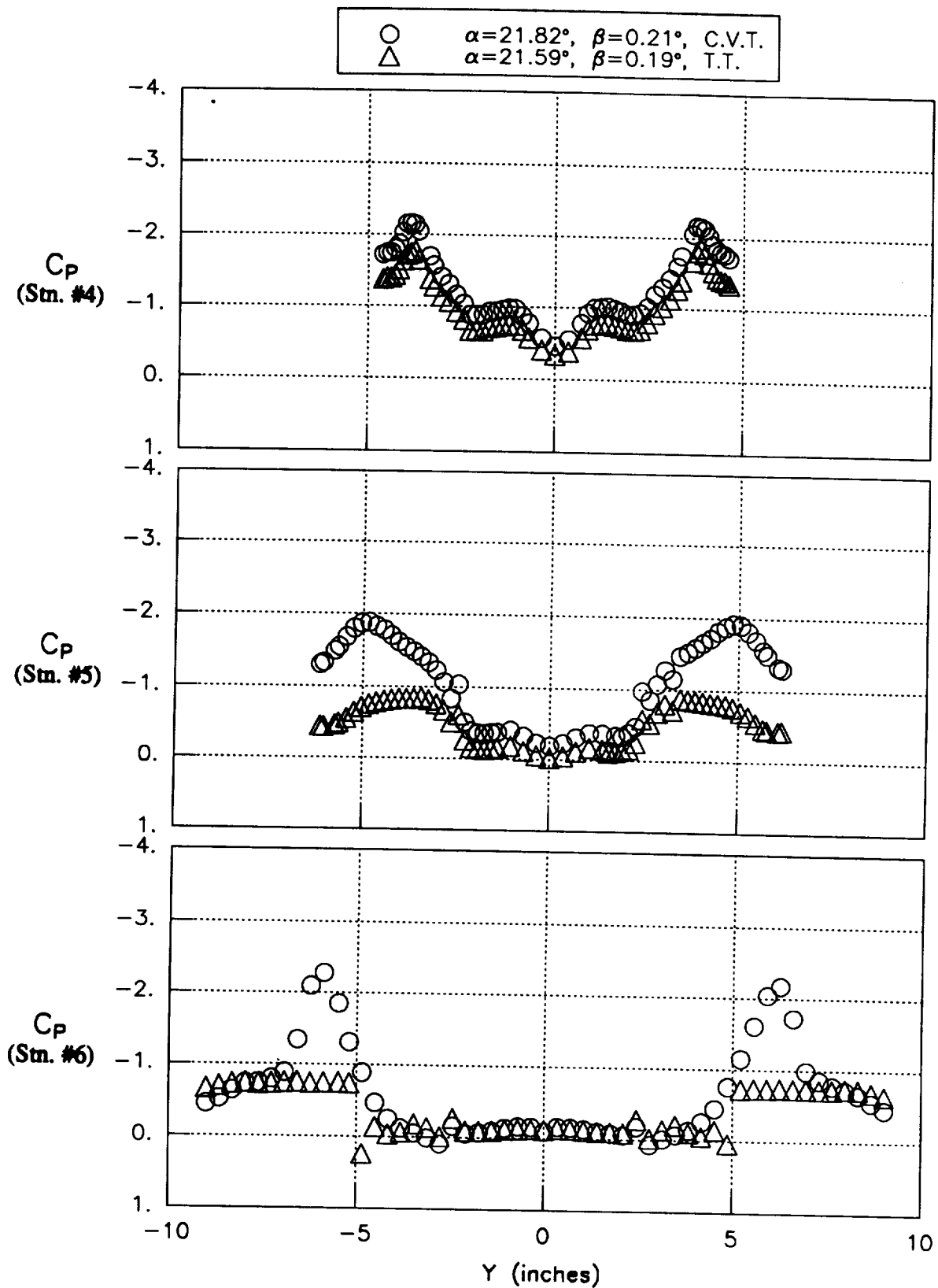
Fig. 7A    Spanwise wing pressure distributions at α = 22°; comparison of central-tail and twin-tail with 0° LEF, M∞ = 0.4.

22
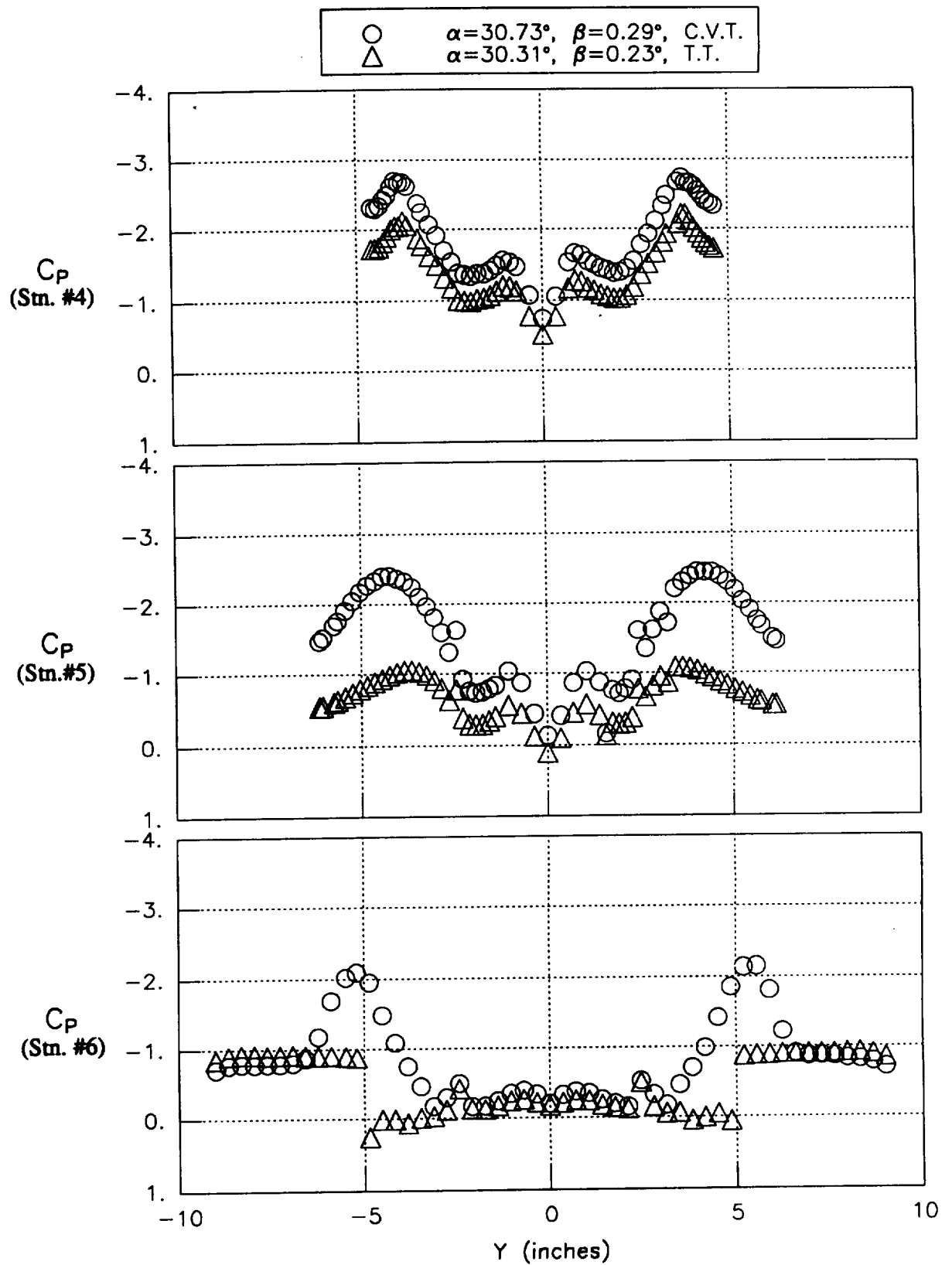
**Fig. 7B**  Spanwise wing pressure distributions at α = 30°; comparison of central-tail and twin-tail with 0° LEF, M∞ = 0.4.
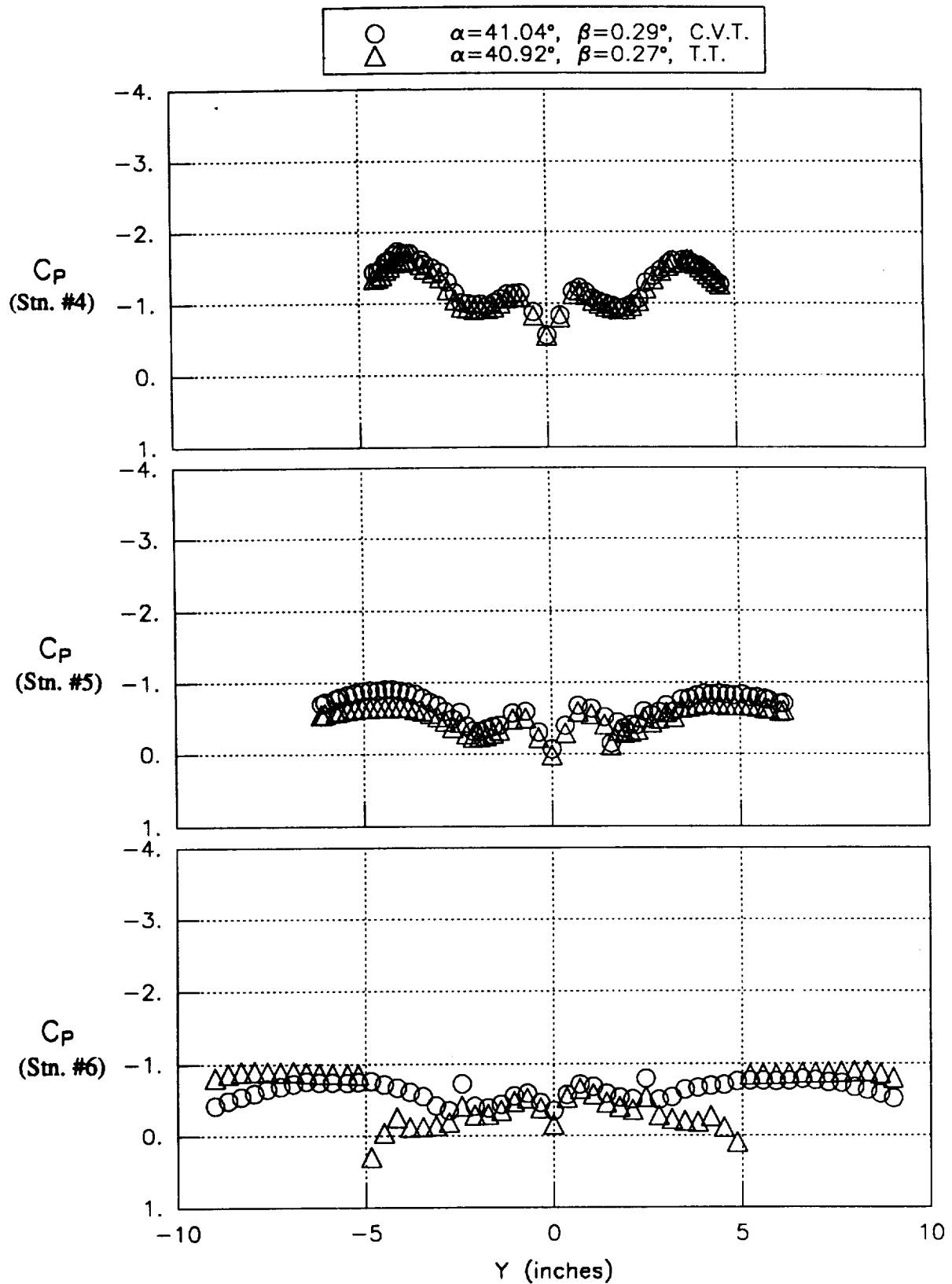
Fig. 7C  Spanwise wing pressure distributions at $\alpha$ = 41°; comparison of central-tail and twin-tail with 0° LEF, $M_\infty$ = 0.4.
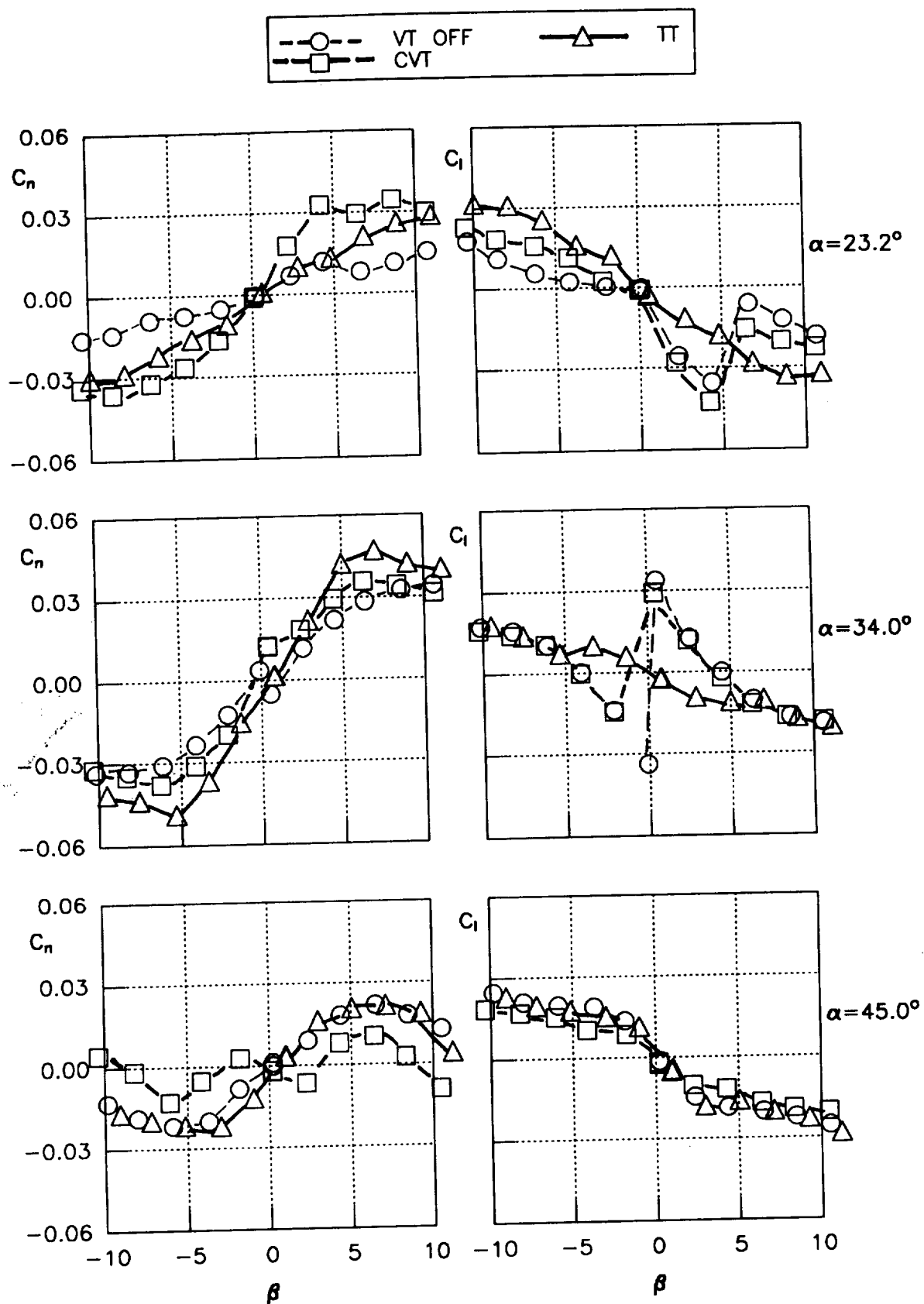
Fig. 8    Yawing and rolling moments versus sideslip at various angles of attack; comparison of central-tail and twin-tail with 0° LEF, $M_\bullet = 0.4$.
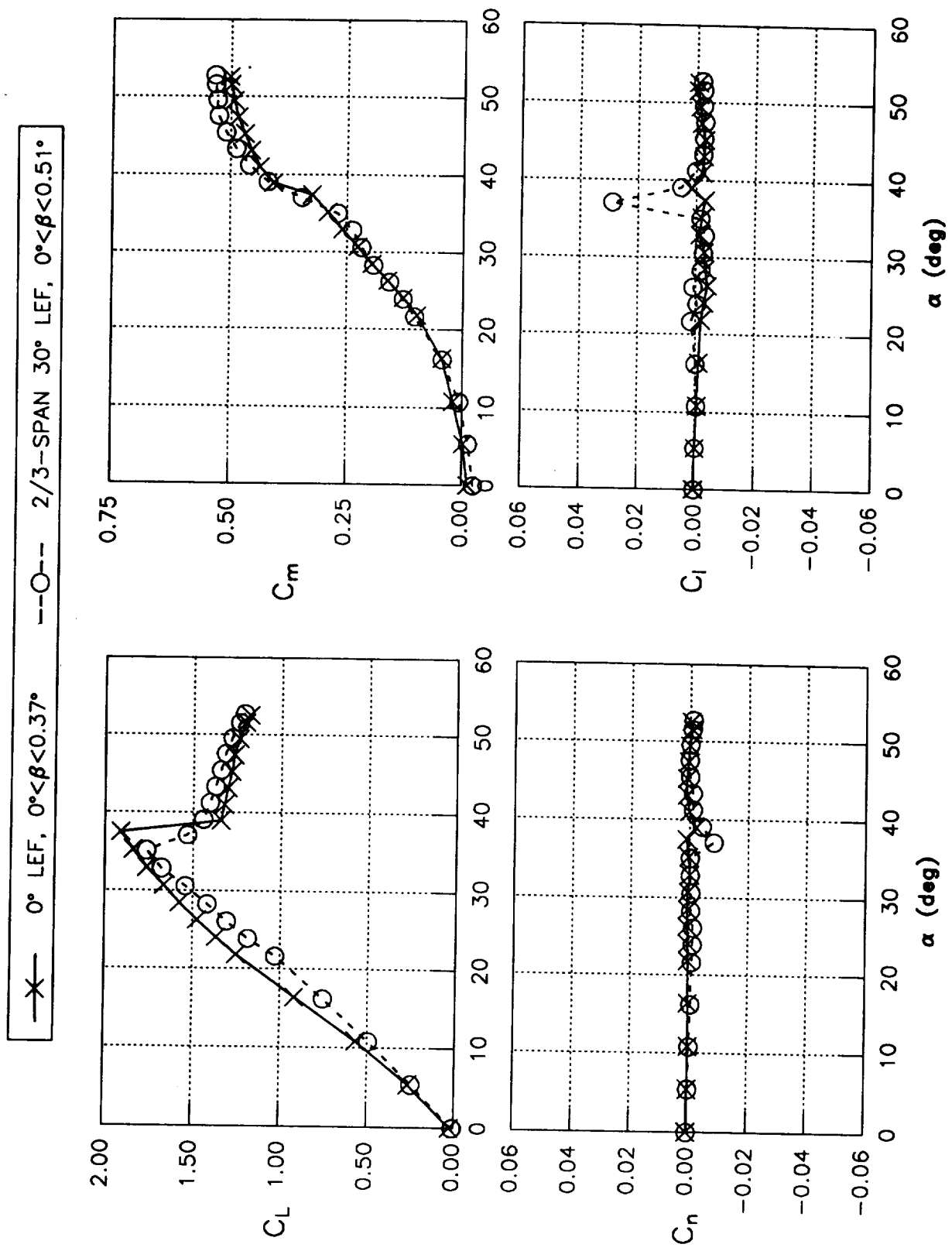
Fig. 9  Lift and moment coefficients versus angle of attack; comparison of 0° LEF and 2/3-span 30° LEF on tail-off configuration, $M_\infty = 0.4$.
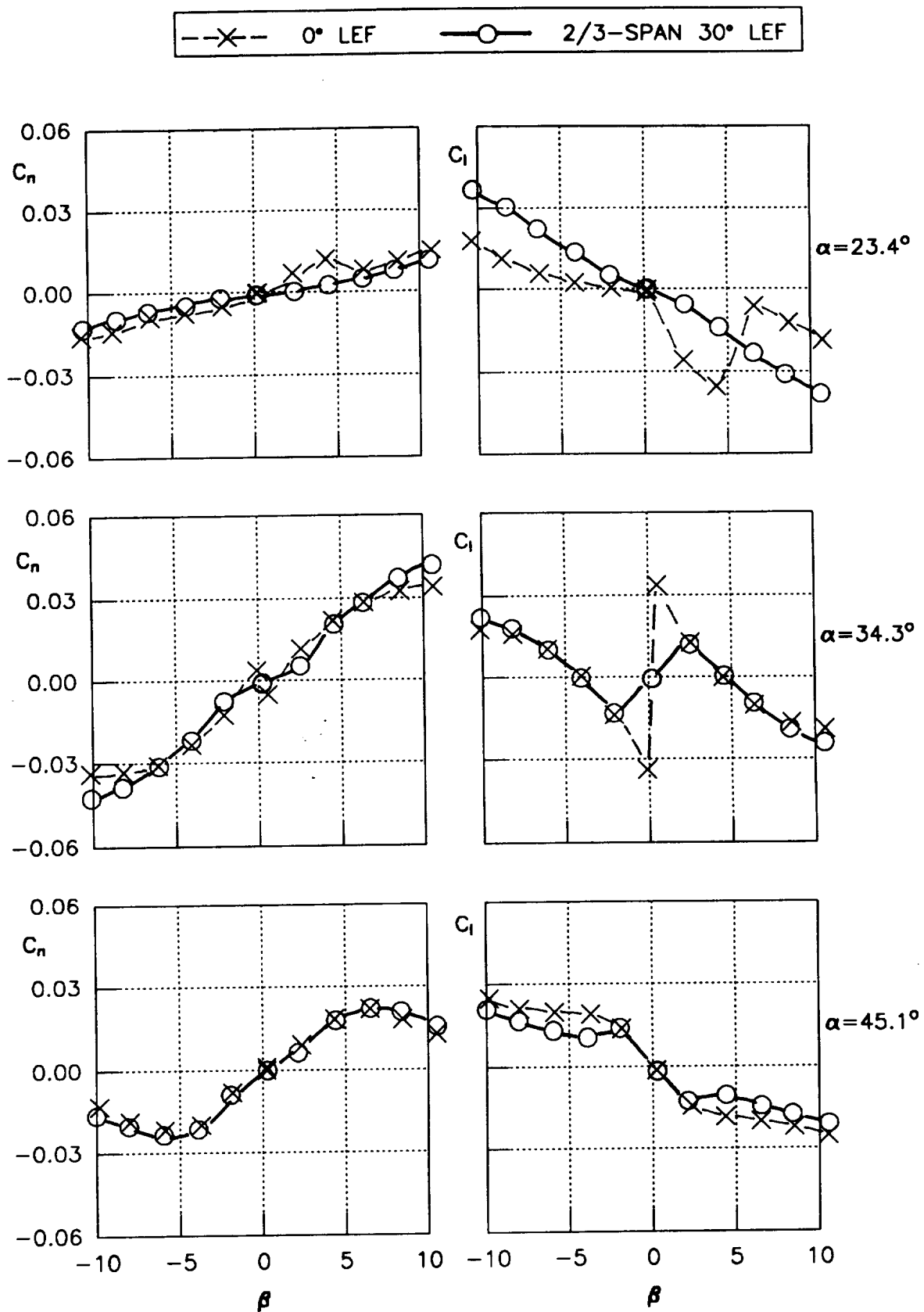
Fig. 10    Yawing and rolling moments versus sideslip at various angles of attack; comparison of 0° LEF and 2/3-span 30° LEF on tail-off configuration, $M_\infty = 0.4$.
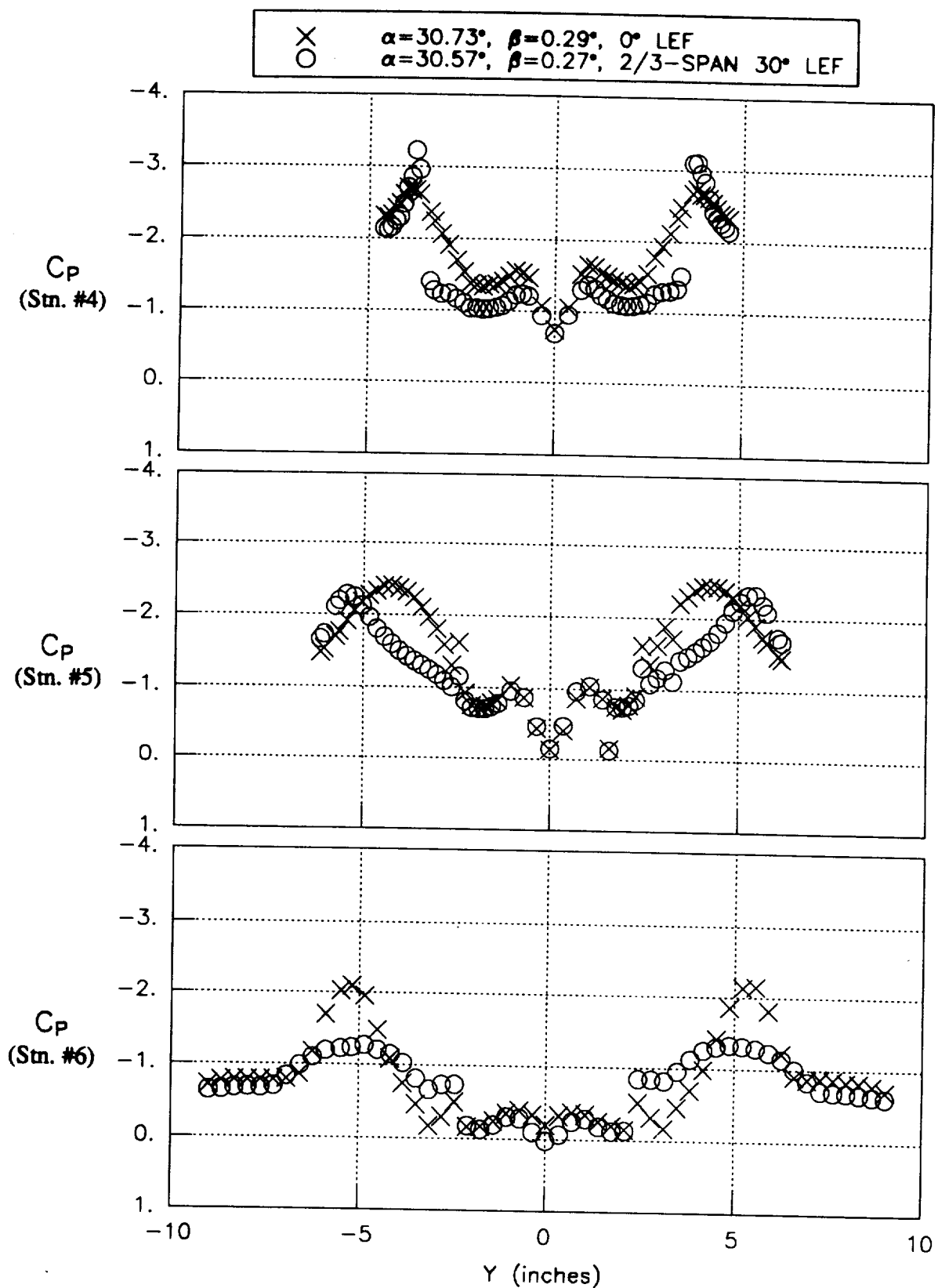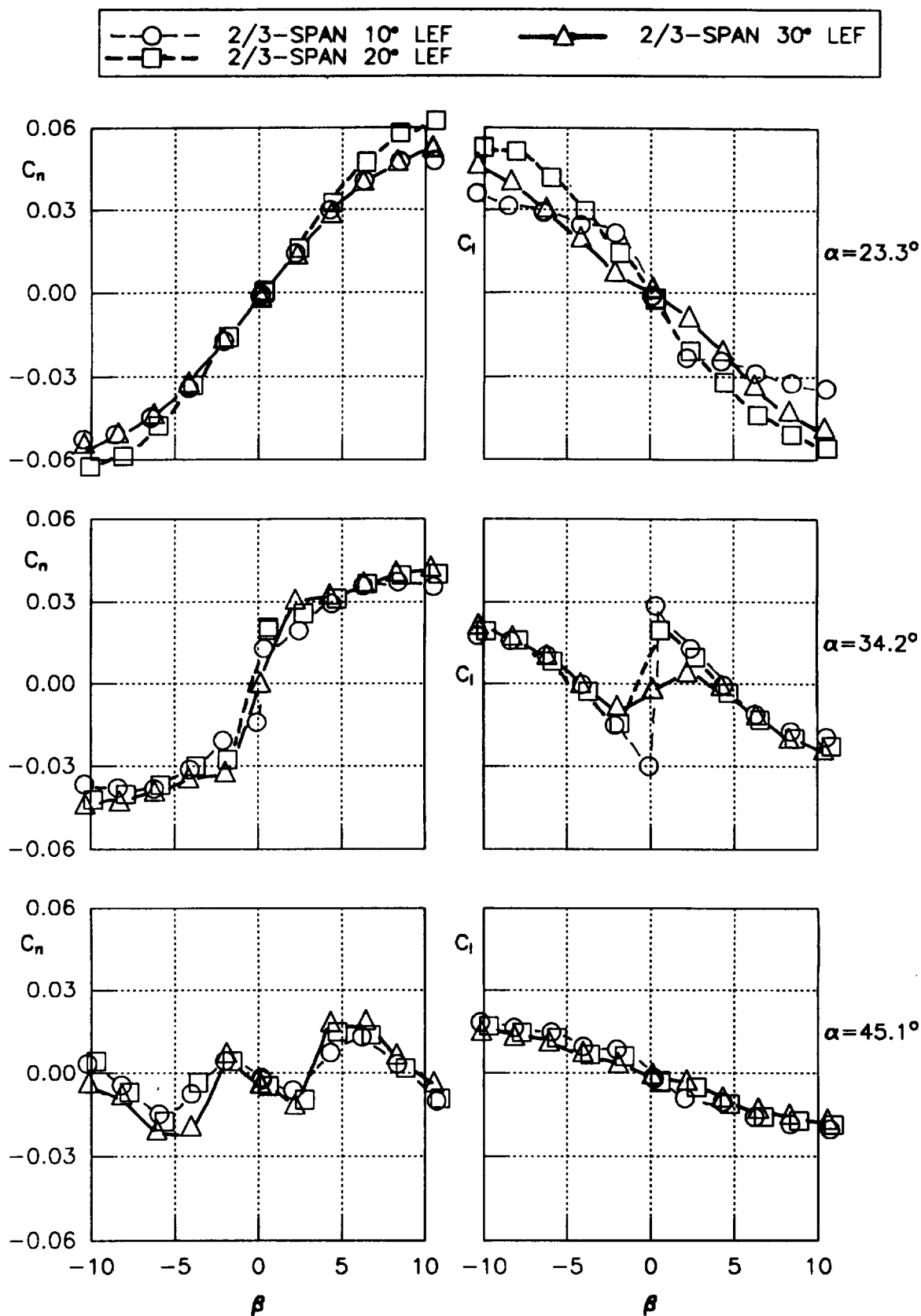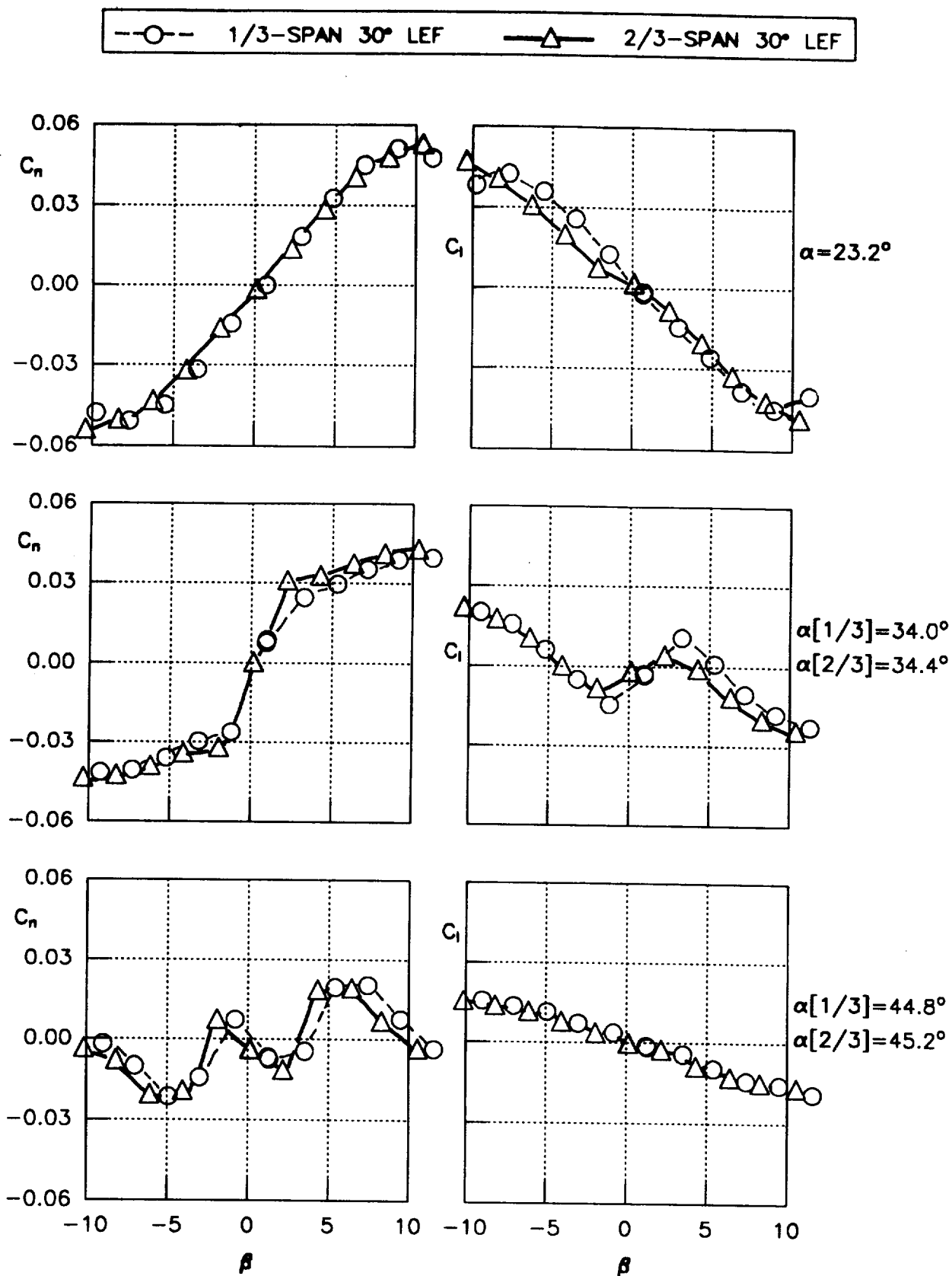
Fig. 11   Spanwise wing pressure distributions at α = 30°; comparison of 0° LEF and 2/3-span 30° LEF on central-tail configuration, M∞ = 0.4.

28
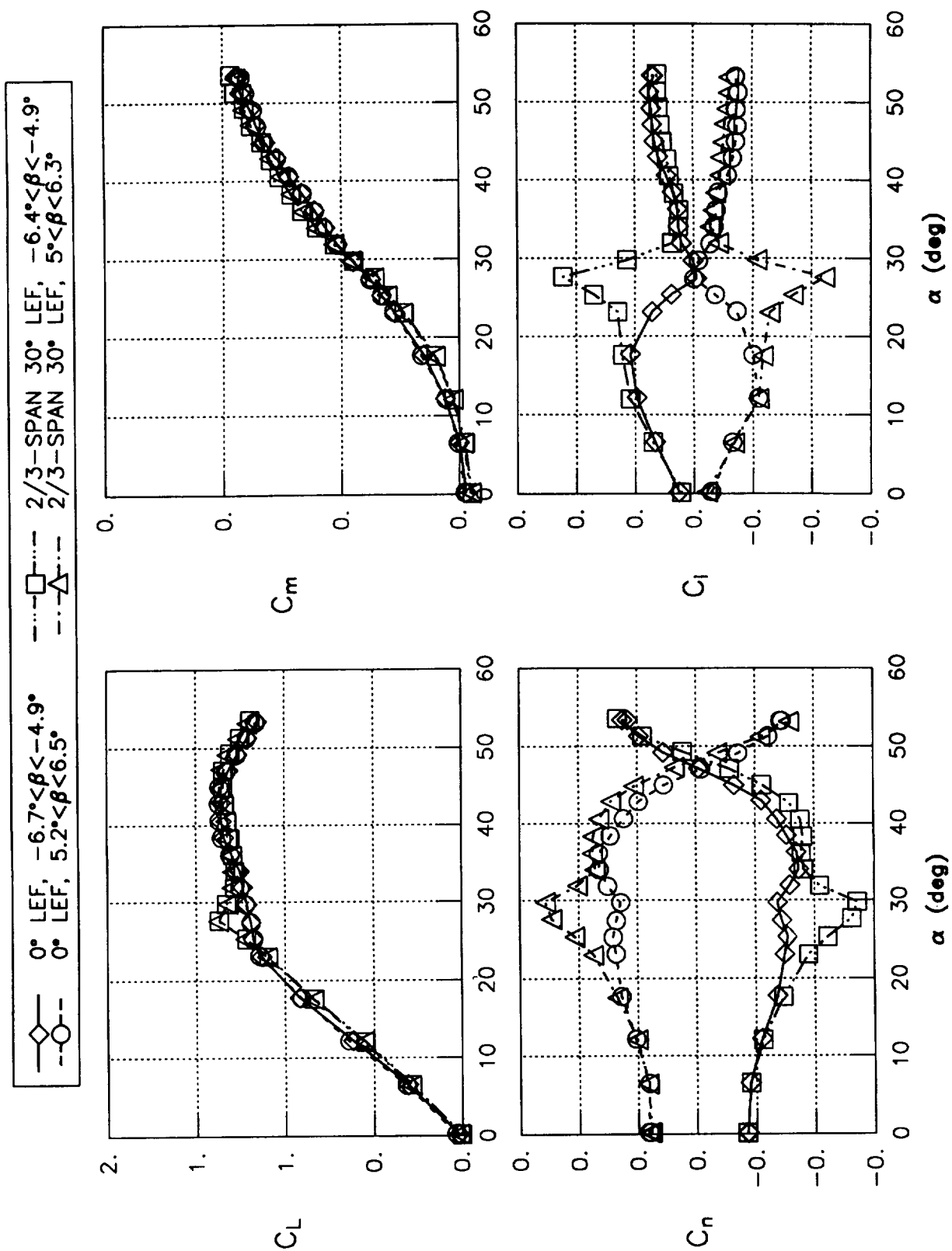
Fig. 12 Lift and moment coefficients versus angle of attack at $\beta = \pm 5°$; comparison of 0° LEF and 2/3-span 30° LEF on the central-tail configuration, $M_\infty = 0.4$.

29
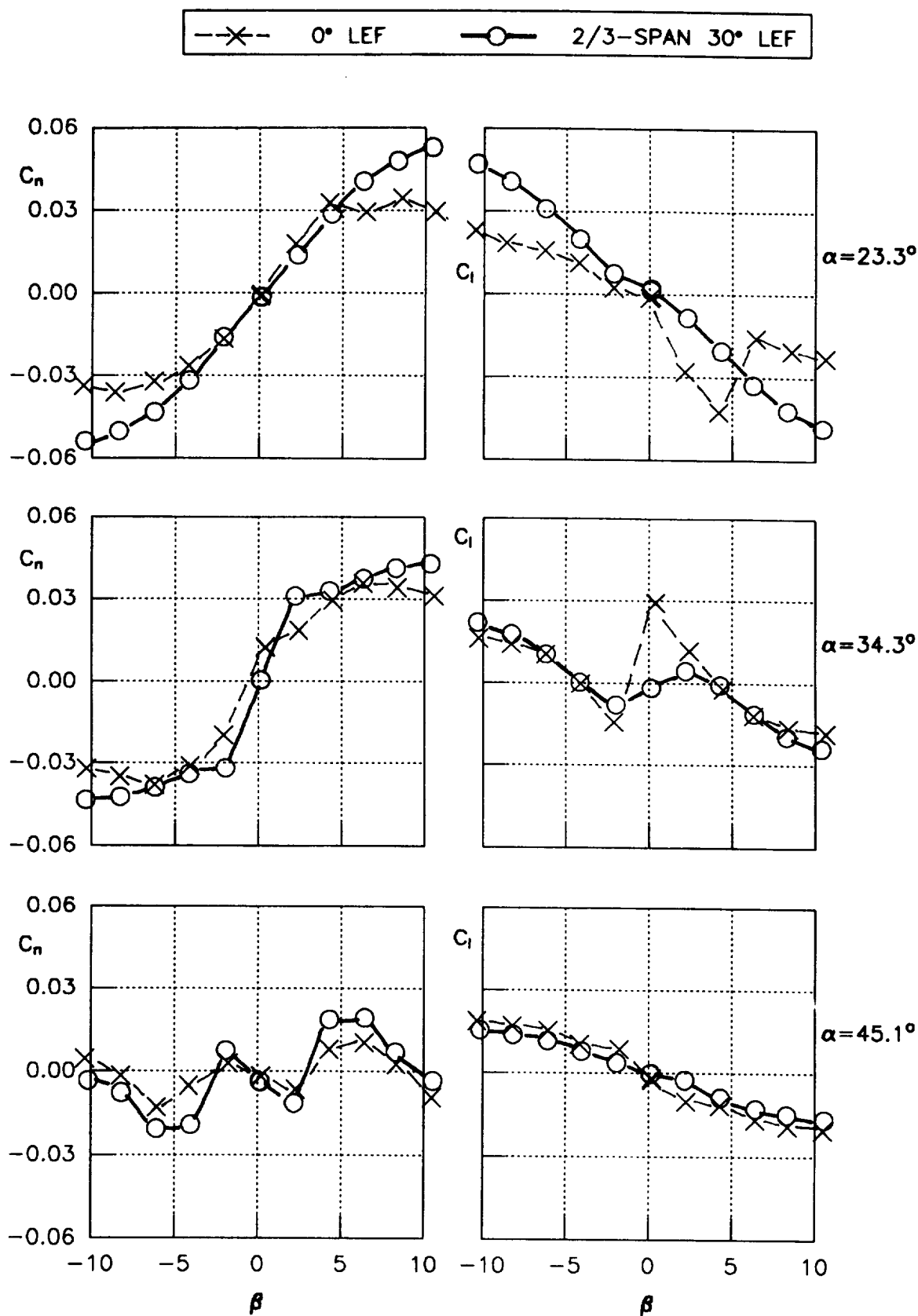
**Fig. 13** Yawing and rolling moments versus sideslip at various angles of attack; comparison of 0° LEF and 2/3-span 30° LEF on central-tail configuration, $M_\infty$ = 0.4.
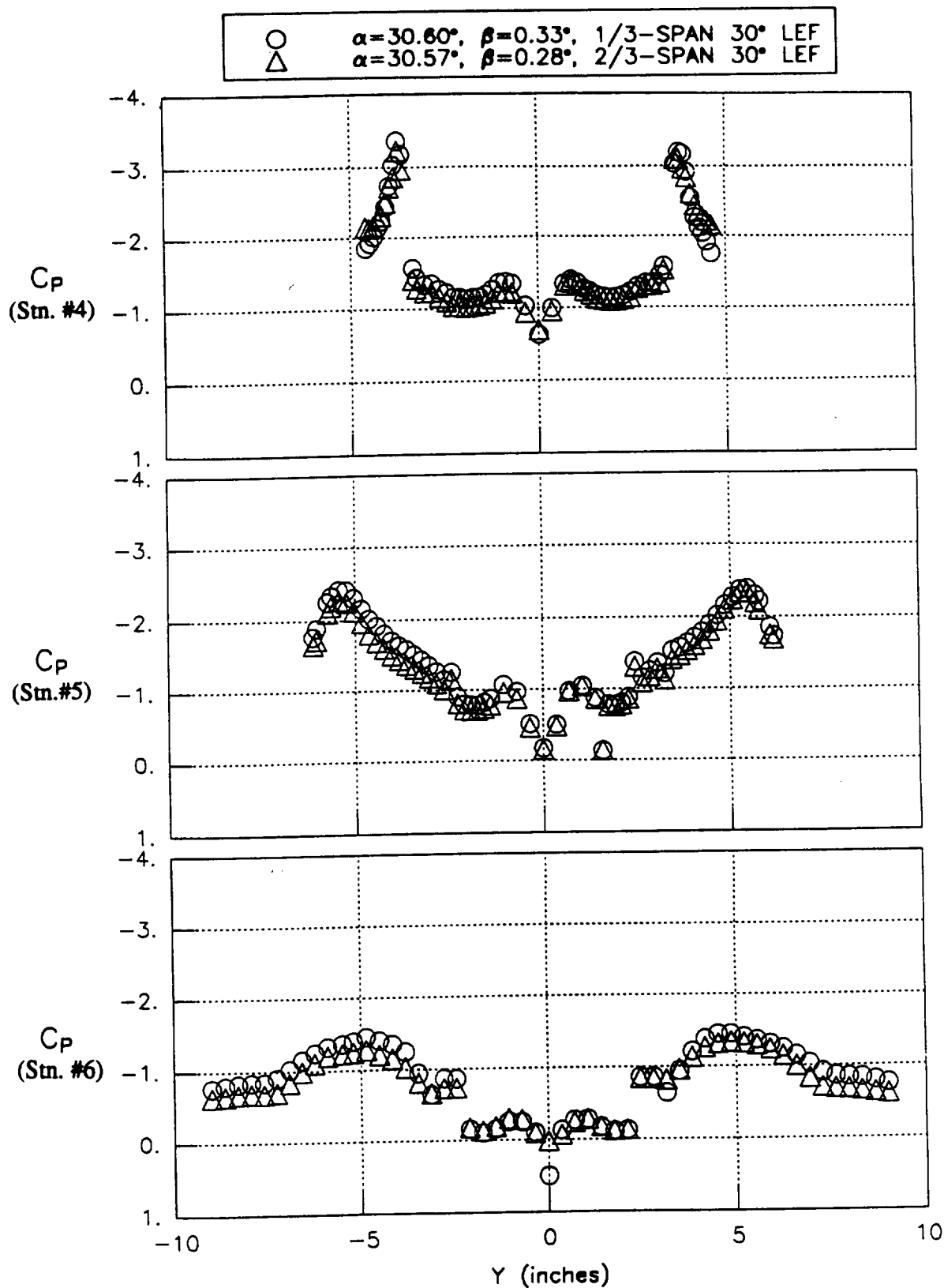
Fig. 14    Yawing and rolling moments versus sideslip at various angles of attack; comparison of 10°, 20° and 30° deflection of 2/3-span LEF on central-tail configuration, $M_\infty$ = 0.4.

Fig. 15    Yawing and rolling moments versus sideslip at various angles of attack;
comparison of 1/3-span and 2/3-span LEF at 30° deflection on central-tail
configuration, $M_\infty$ = 0.4.

Fig. 16    Spanwise wing pressure distributions at $\alpha = 30°$; comparison of 1/3-span and 2/3-span LEF at 30° deflection on central-tail configuration, $M_\infty = 0.4$.

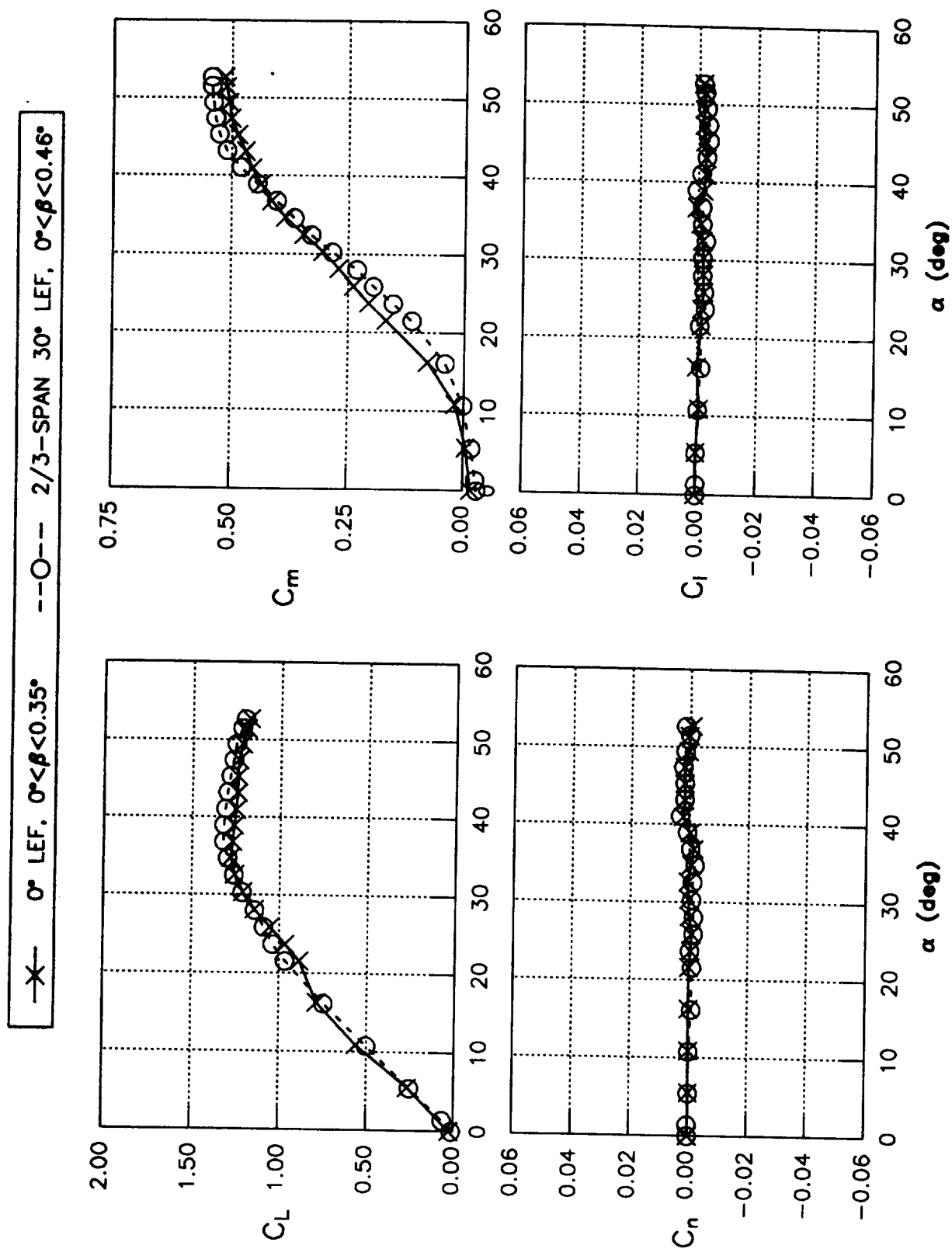Fig. 17 Lift and moment coefficients versus angle of attack; comparison of 0° LEF and 2/3-span 30° LEF on twin-tail configuration, $M_\infty = 0.4$.
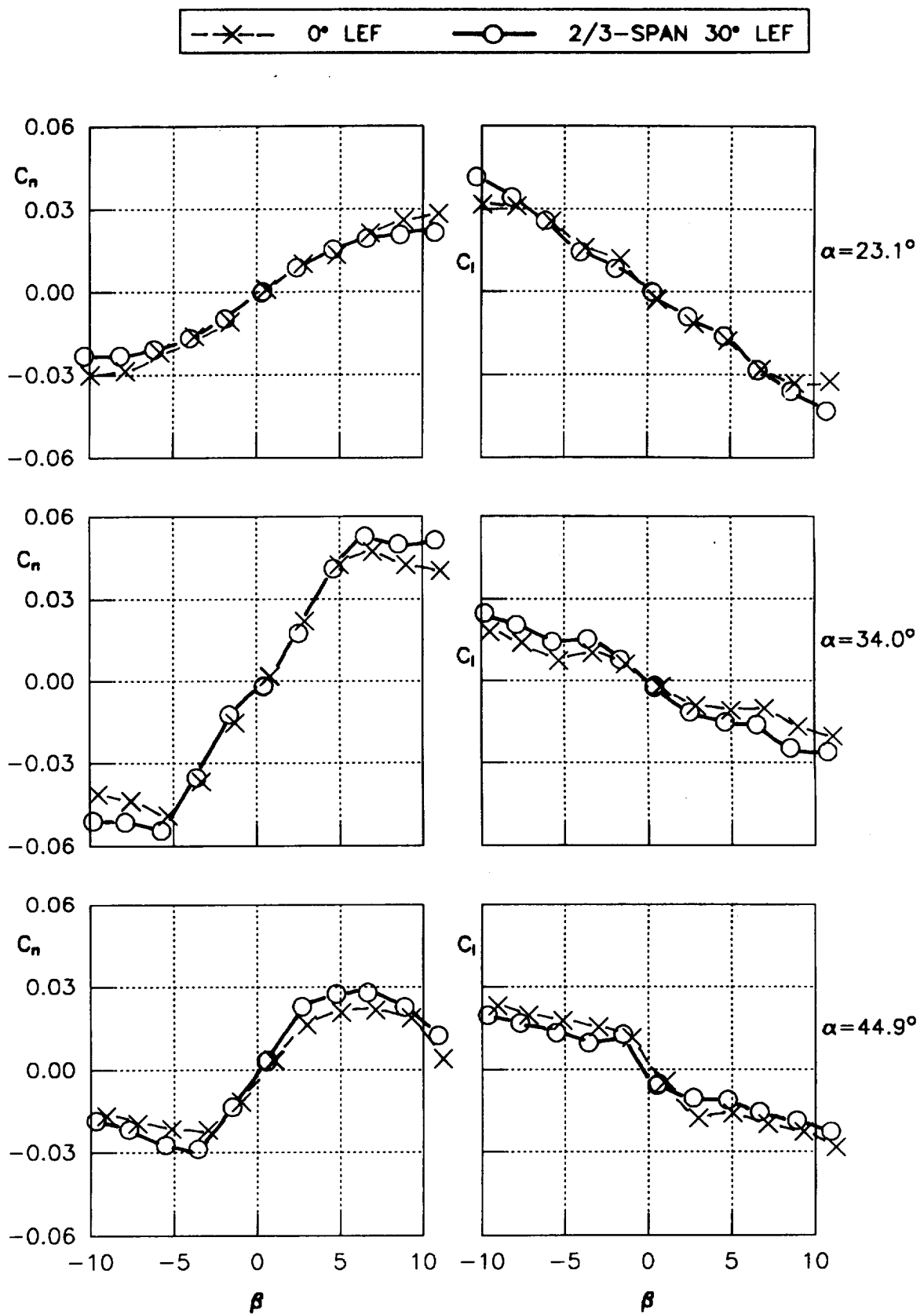
34

**Fig. 18** Yawing and rolling moments versus sideslip at various angles of attack; comparison of 0° LEF and 2/3-span LEF at 30° deflection on twin-tail configuration, $M_\infty = 0.4$.
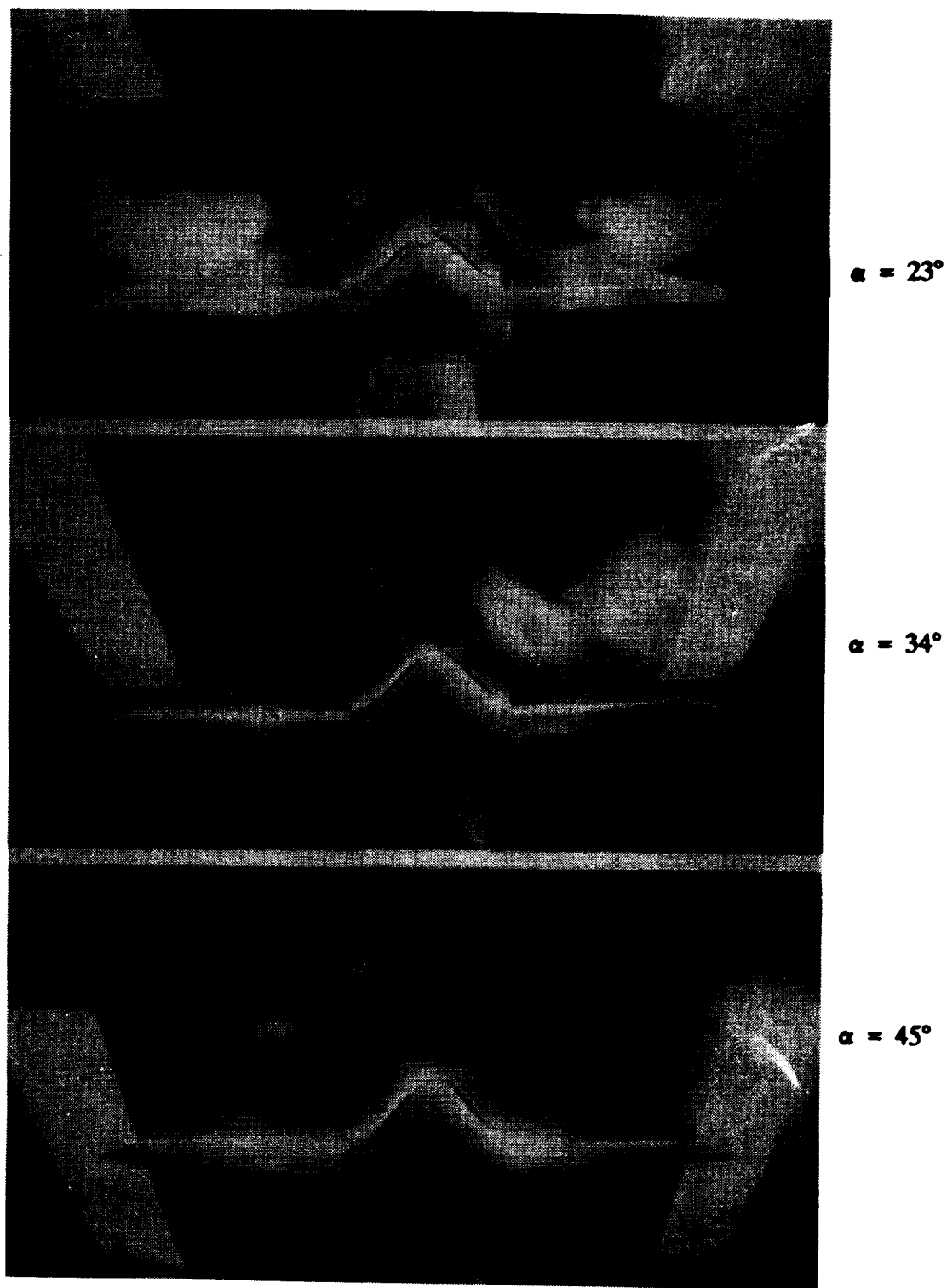
$\alpha = 23°$

$\alpha = 34°$

$\alpha = 45°$

Fig. 19    Flow visualizations various angles of attack on baseline (tail off, 0° LEF) configuration, $M_\infty = 0.4$.
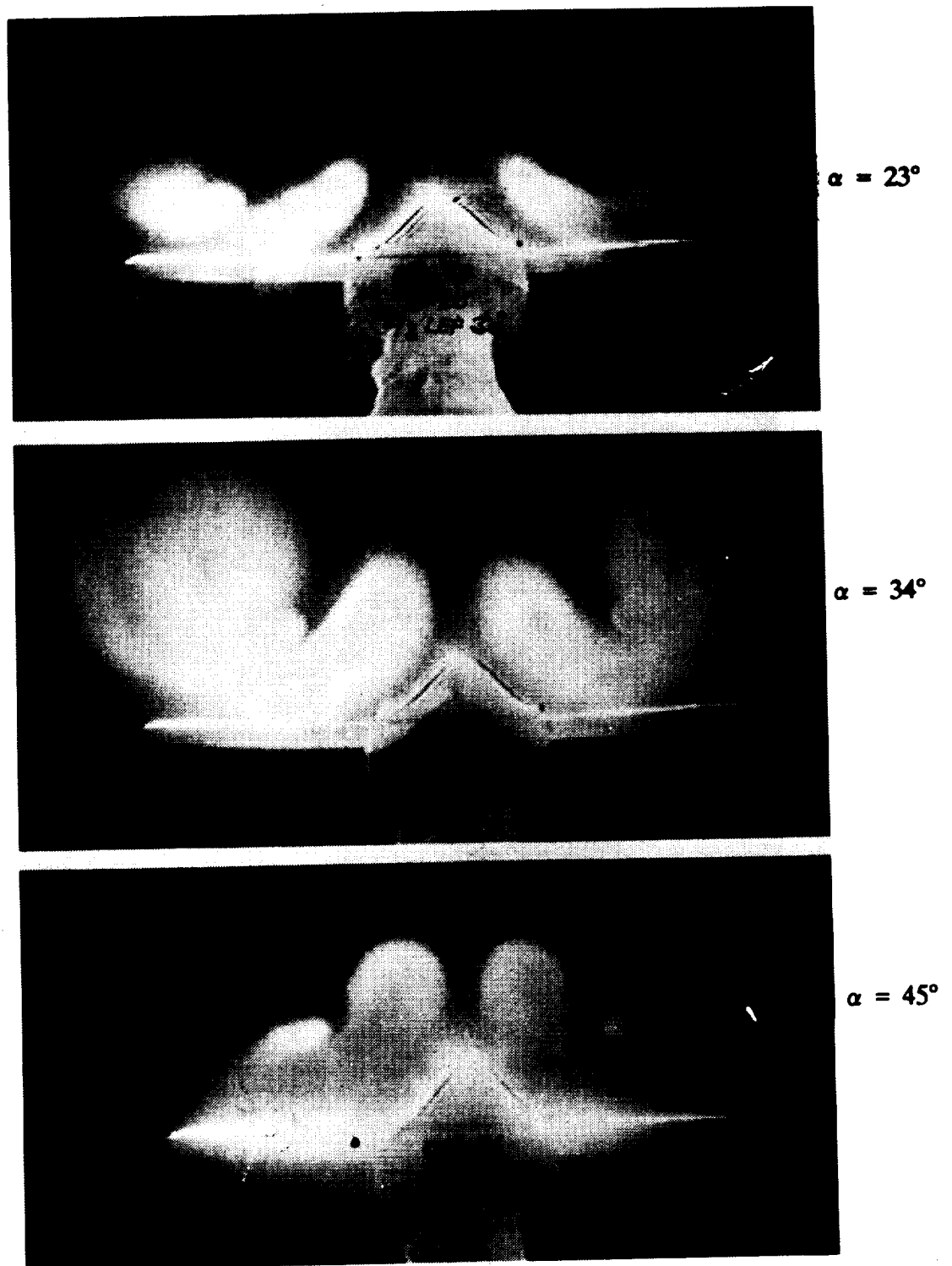
$\alpha = 23°$

$\alpha = 34°$

$\alpha = 45°$

Fig. 20    Flow visualizations at various angles of attack on tail off configuration with 2/3-span LEF at 30° deflection, $M_\infty = 0.4$.

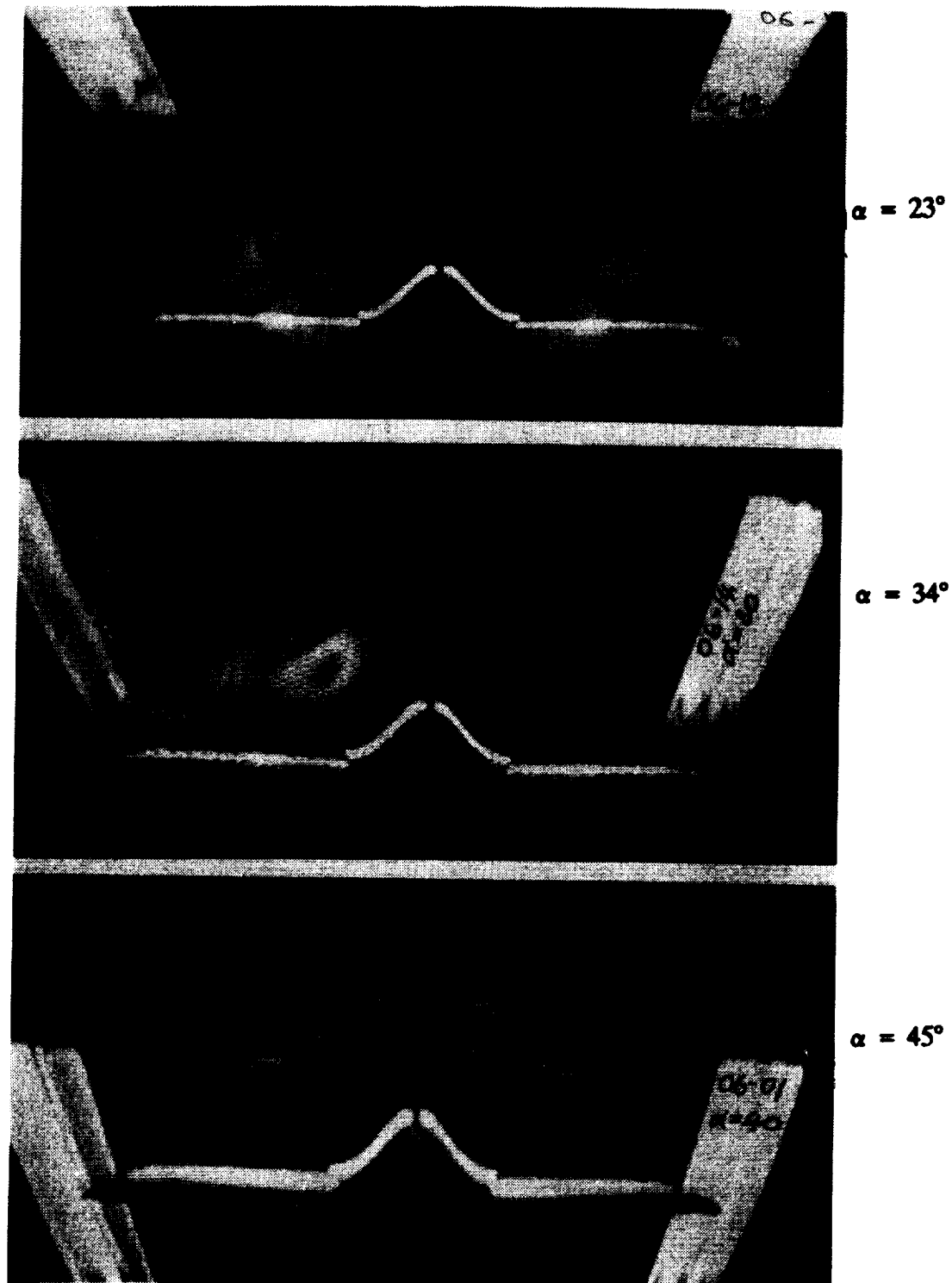$\alpha = 23°$

$\alpha = 34°$

$\alpha = 45°$

**Fig. 21**    Flow visualizations at various angles of attack on central-tail configuration, $0°$ LEF, $M_\infty = 0.4$.

$\alpha = 23°$

$\alpha = 34°$

$\alpha = 45°$

Fig. 22    Flow visualizations at various angles of attack on central-tail configuration with 2/3-span LEF at 30° deflection, $M_\infty = 0.4$.

$\alpha = 23°$

$\alpha = 34°$

$\alpha = 45°$
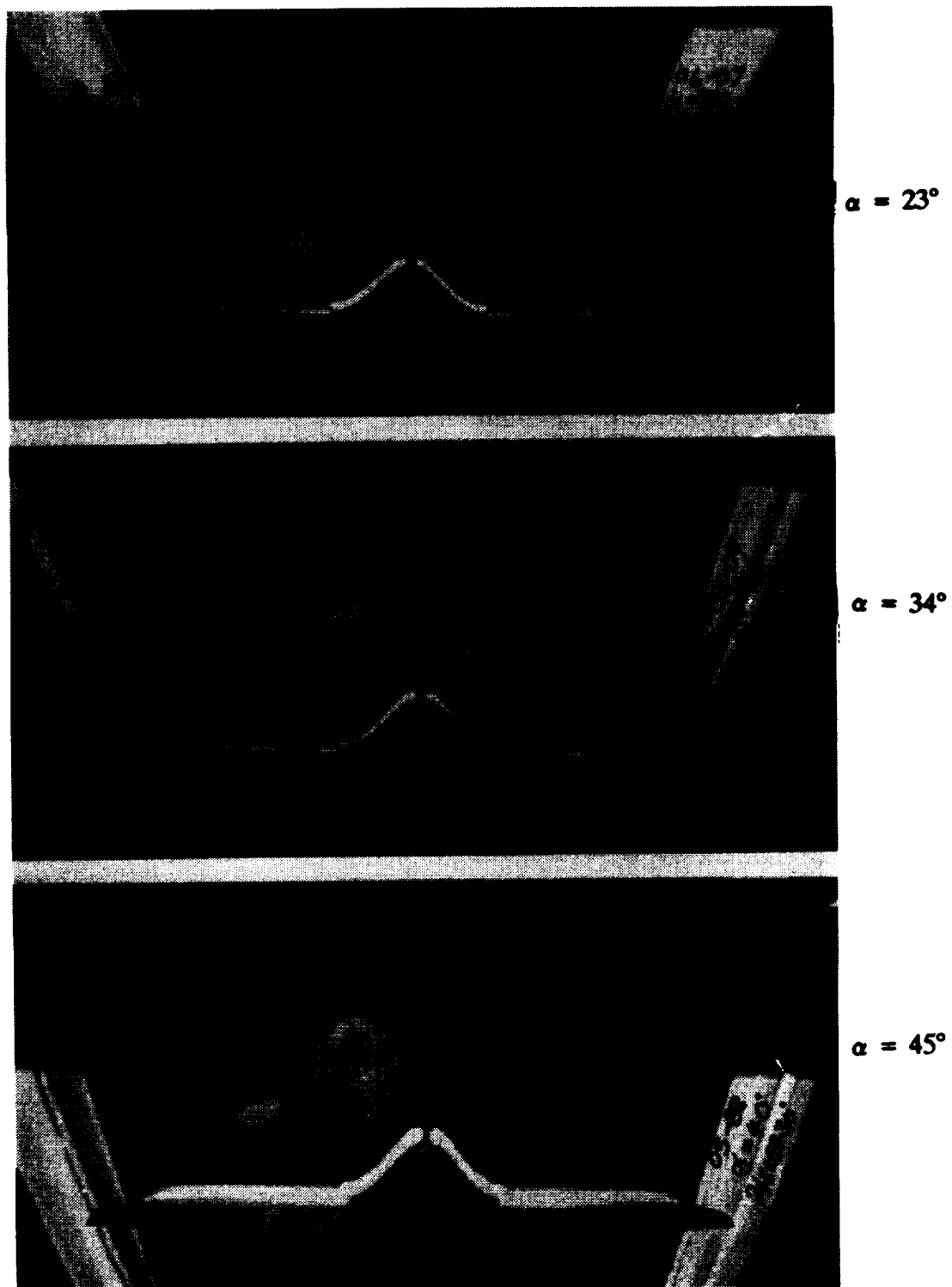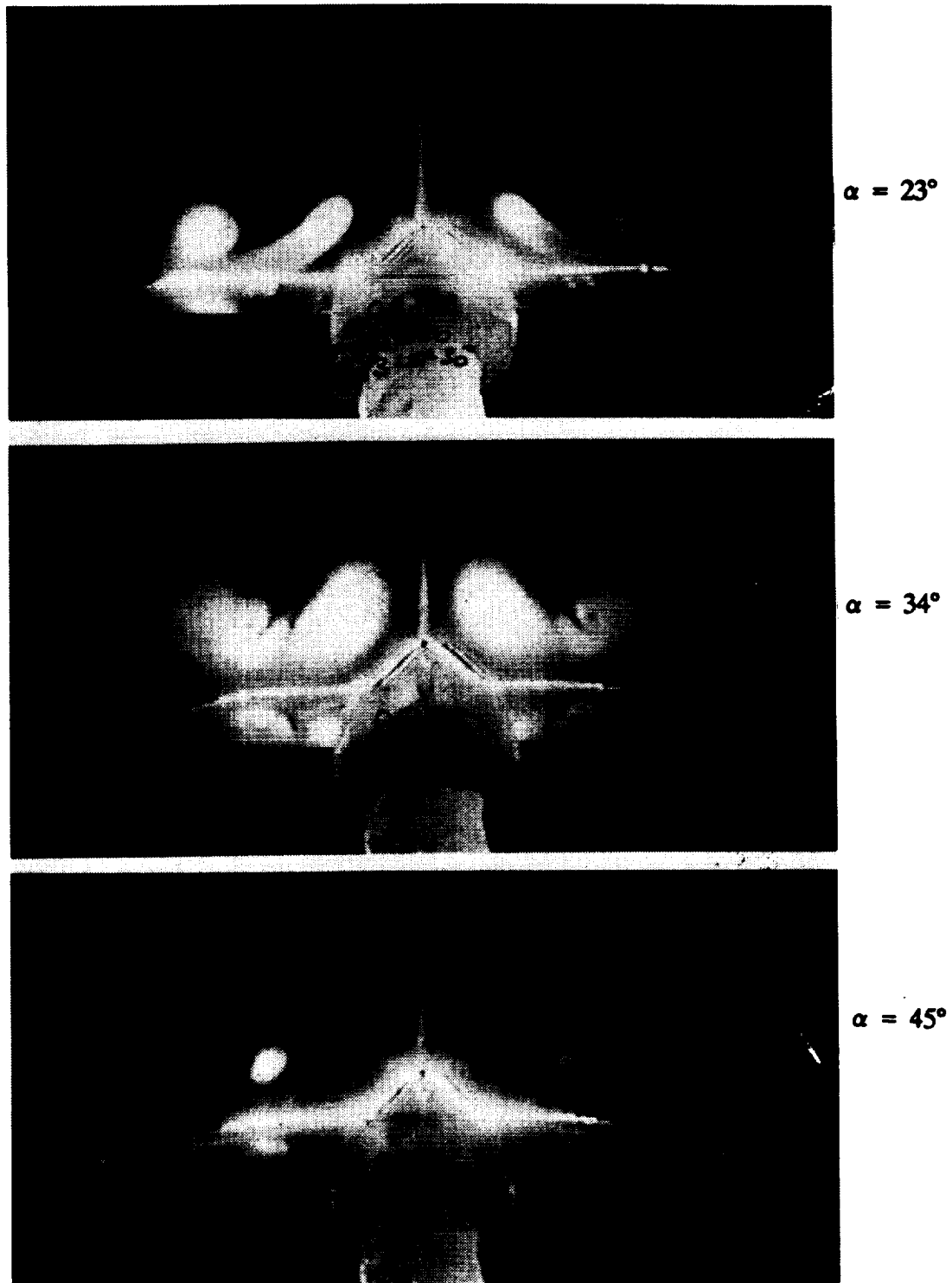
Fig. 23    Flow visualizations at various angles of attack on central-tail configuration with 1/3-span LEF at 30° deflection, $M_\infty = 0.4$.

0° LEF

2/3-span
30° LEF
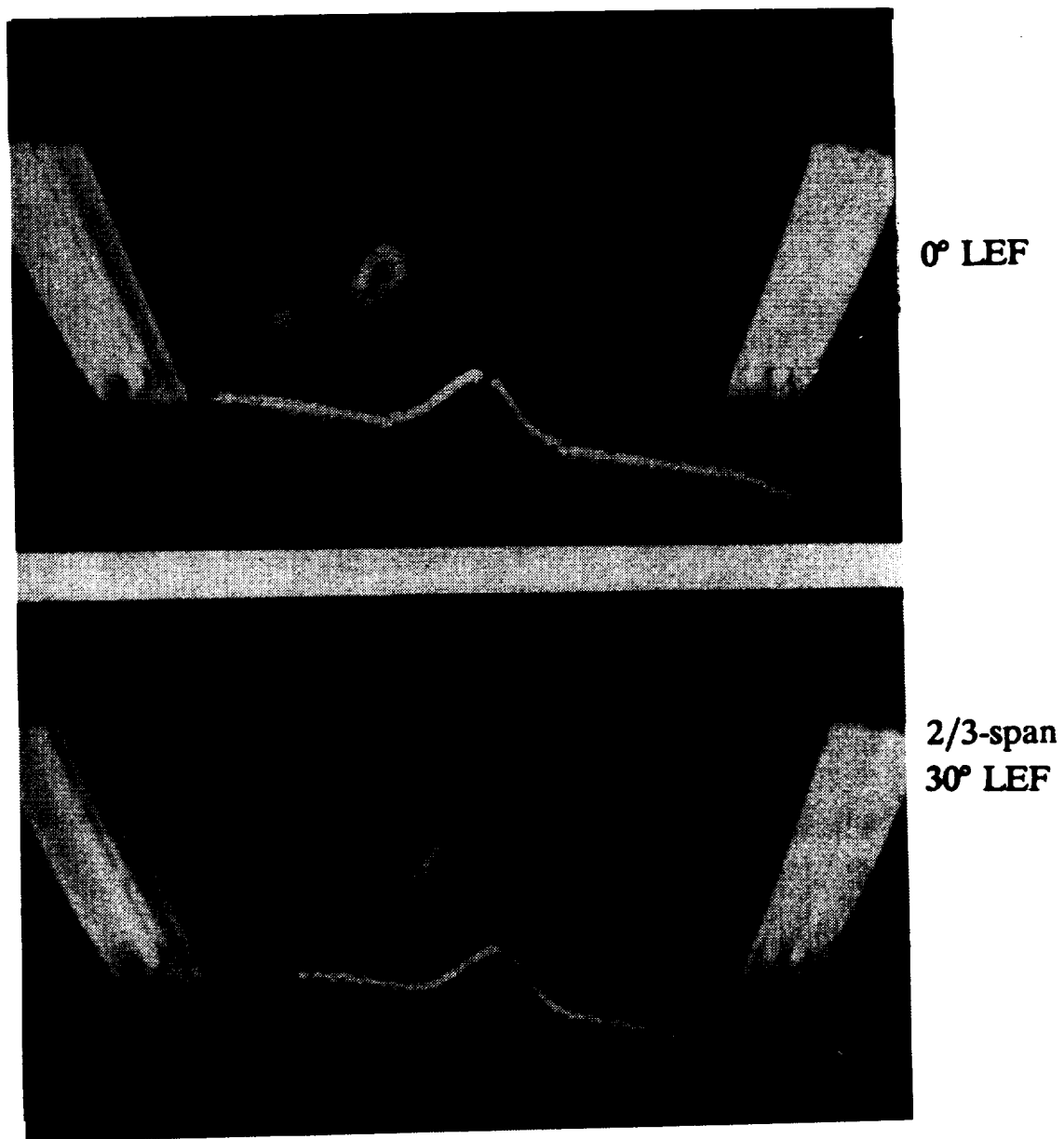
Fig. 24     Flow visualizations at $\alpha$ = 34° and ß = 4° on central-tail configuration; comparing 0° LEF and 2/3-span LEF at 30° deflection, $M_\infty$ = 0.4.

41

$\alpha = 23°$

$\alpha = 34°$

$\alpha = 45°$
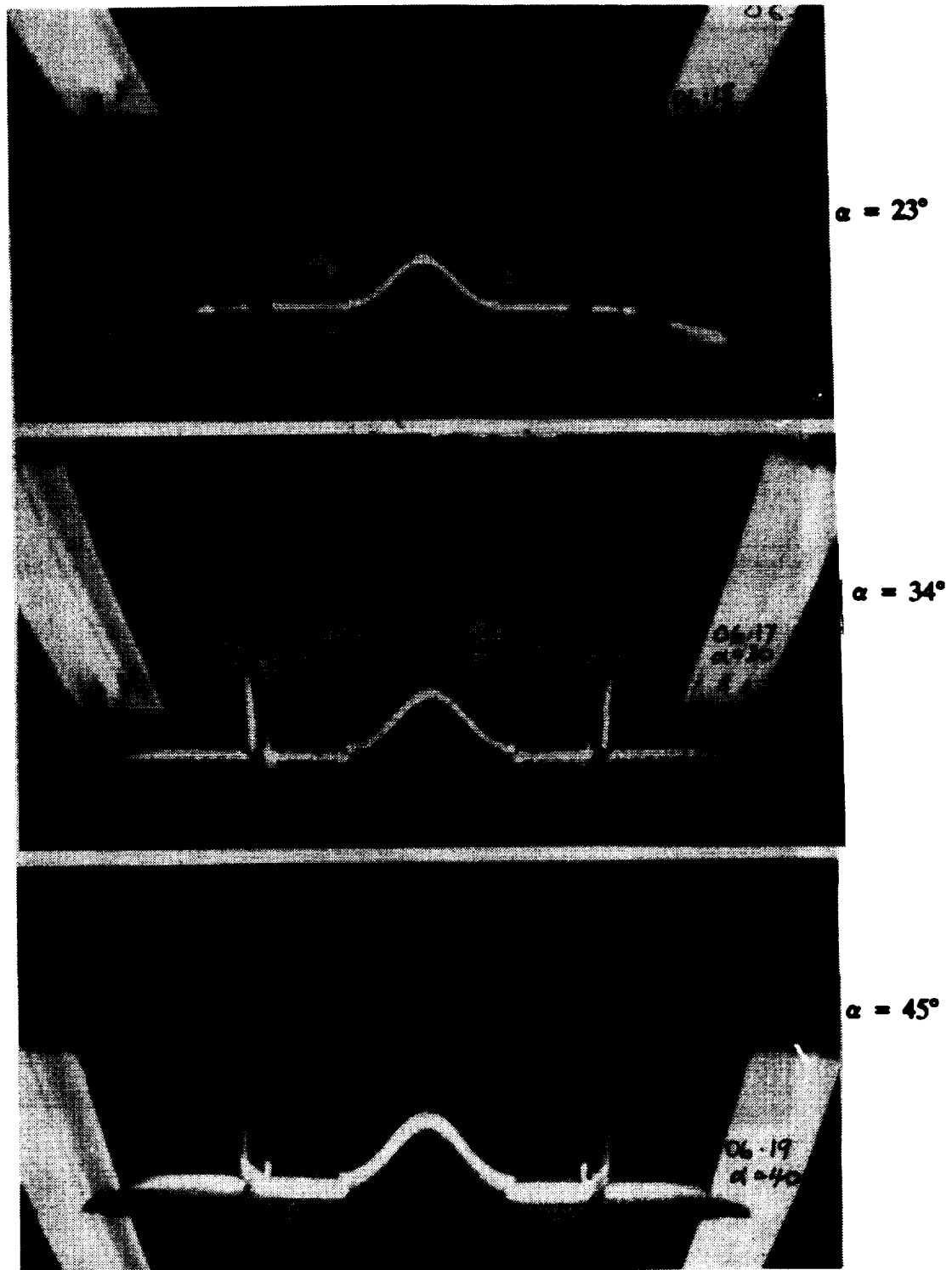
**Fig. 25**    Flow visualizations at various angles of attack on twin-tail configuration, 0° LEF, $M_\infty = 0.4$.
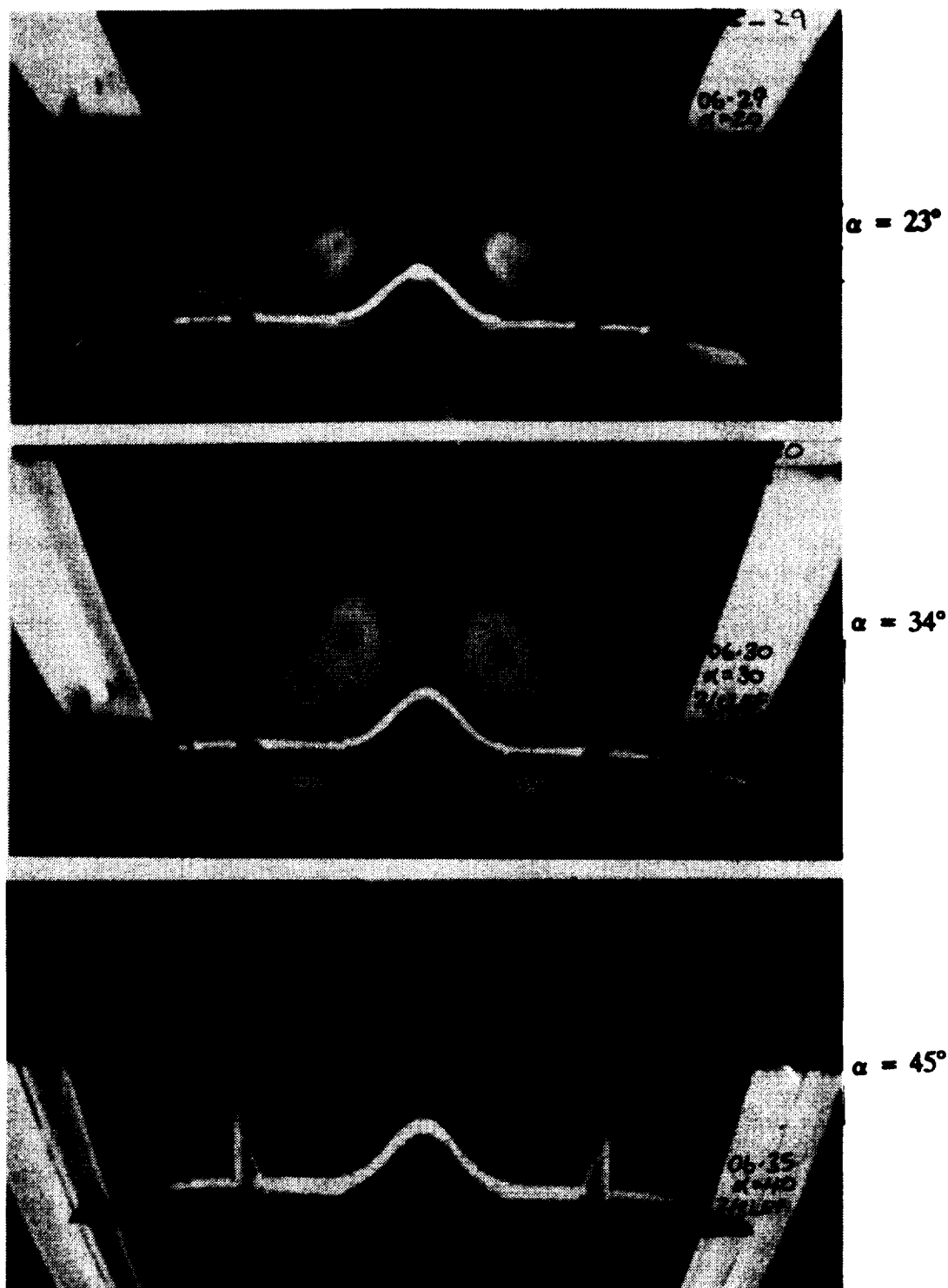
α = 23°

α = 34°

α = 45°

Fig. 26    Flow visualizations at various angles of attack on twin-tail configuration with 2/3-span LEF at 30° deflection, $M_\infty$ = 0.4.

# REPORT DOCUMENTATION PAGE

Public reporting burden for this collection of information is estimated to average 1 hour per response, including the time for reviewing instructions, searching existing data sources, gathering and maintaining the data needed, and completing and reviewing the collection of information. Send comments regarding this burden estimate or any other aspect of this collection of information, including suggestions for reducing this burden, to Washington Headquarters Services, Directorate for Information Operations and Reports, 1215 Jefferson Davis Highway, Suite 1204, Arlington, VA 22202-4302, and to the Office of Management and Budget, Paperwork Reduction Project (0704-0188), Washington, DC 20503.

| 1. AGENCY USE ONLY (Leave blank) | 2. REPORT DATE<br>. April 1992 | 3. REPORT TYPE AND DATES COVERED<br>Contractor Report |
|---|---|---|

| 4. TITLE AND SUBTITLE<br>Subsonic Investigations of Vortex Interaction Control For Enhanced High-Alpha Aerodynamics of A Chine Forebody/ Delta Wing Configuration | 5. FUNDING NUMBERS<br>C NAS1-18856<br>WU 505-68-30-03 |
|---|---|
| 6. AUTHOR(S)<br>Dhanvada M. Rao and M. K. Bhat | |

| 7. PERFORMING ORGANIZATION NAME(S) AND ADDRESS(ES)<br>ViGYAN Inc.<br>30 Research Drive<br>Hampton, Virginia 23666-1325 | 8. PERFORMING ORGANIZATION REPORT NUMBER |
|---|---|

| 9. SPONSORING/MONITORING AGENCY NAME(S) AND ADDRESS(ES)<br>National Aeronautics and Space Administration<br>Langley Research Center<br>Hampton, Virginia 23666-5225 | 10. SPONSORING/MONITORING AGENCY REPORT NUMBER<br>NASA CR-189641 |
|---|---|

**11. SUPPLEMENTARY NOTES**

NASA Langley Reserach Center, Technical Monitor: Robert M. Hall

| 12a. DISTRIBUTION/AVAILABILITY STATEMENT<br>Unclassified - Unlimited<br>Subject Category 02 | 12b. DISTRIBUTION CODE |
|---|---|

**13. ABSTRACT (Maximum 200 words)**

A proposed concept to alleviate high-alpha asymmetry and lateral/directional instability by decoupling of forebody and wing vortices was investigated on a generic chine forebody/ 60 deg. delta configuration in the NASA Langley 7- by 10-Foot High Speed Tunnel. The decoupling technique involved inboard leading-edge flaps of varying span and deflection angle. Six-component force/moment characteristics, surface pressure distributions and vapor-screen flow visualizations were acquired, on the basic wing-body configuration and with both single and twin vertical tails at $M_\infty = 0.1$ and $0.4$, and in the range $\alpha = 0^\delta$ to $50^\circ$ and $\beta = -10^\circ$ to $+10^\circ$. This report presents results highlighting the potential of vortex decoupling via leading-edge flaps for enhanced high-alpha lateral/directional characteristics.

| 14. SUBJECT TERMS<br>High-Alpha Aerodynamics Vortex Control | 15. NUMBER OF PAGES<br>44 |
|---|---|
| | 16. PRICE CODE<br>A03 |

| 17. SECURITY CLASSIFICATION OF REPORT<br>Unclassified | 18. SECURITY CLASSIFICATION OF THIS PAGE<br>Unclassified | 19. SECURITY CLASSIFICATION OF ABSTRACT<br>Unclassified | 20. LIMITATION OF ABSTRACT |
|---|---|---|---|

NSN 7540-01-280-5500